Journal of Medicinal Chemistry

Article

Bio-Inspired Dual Selective BCL-2/c-MYC G-Quadruplex Binders: Design, Synthesis and Anticancer Activity of Drug-like Imidazo[2,1-i]purine Derivatives.

Sveva Pelliccia, Jussara Amato, Domenica Capasso, Sonia Di Gaetano, Alberto Massarotti, Marialuisa Piccolo, Carlo Irace, Gian Cesare Tron, Bruno Pagano, Antonio Randazzo, Ettore Novellino, and Mariateresa Giustiniano

J. Med. Chem., **Just Accepted Manuscript** • DOI: 10.1021/acs.jmedchem.9b00262 • Publication Date (Web): 26 Jun 2019

Just Accepted

Bio-Inspired Dual Selective *BCL-2*/*c-MYC* G-Quadruplex Binders: Design, Synthesis and Anticancer Activity of Drug-like Imidazo[2,1-*i*]purine Derivatives.

Sveva Pelliccia,[†,#] Jussara Amato,[†,#] Domenica Capasso,[†] Sonia Di Gaetano,[‡] Alberto Massarotti,[§] Marialuisa Piccolo,[†] Carlo Irace,[†] Gian Cesare Tron,[§] Bruno Pagano,[†] Antonio Randazzo,[†] Ettore Novellino,[†] and Mariateresa Giustiniano*[,†].

† Department of Pharmacy, University of Naples "Federico II", Via D. Montesano 49, 80131, Naples, Italy

‡ Institute of Biostructures and Bioimaging, CNR, Via Mezzocannone 16, 80134, Naples, Italy

§ Department of Pharmaceutical Sciences, University of Piemonte Orientale, Largo Donegani 2, 28100 Novara, Italy

KEYWORDS. G-Quadruplex; BCL2; *c*-MYC; Groebke-Blackburn-Bienaymé Reaction; Anticancer Drugs

Abstract

In the search for new drug-like selective G-quadruplex binders, a bio-inspired design focused on the use of nucleobases as synthons in a multicomponent reaction has been herein proved to be viable and successful. Hence, a new class of multi-functionalized imidazo[2,1-*i*]purine derivatives, easily synthesized with a convergent approach, allowed for the identification of the first dual *BCL2*/*c-MYC* gene promoter G-quadruplex ligand. Biophysical studies involving CD melting experiments, MST measurements, NMR titrations, and computational docking calculations, as well as biological investigations including cytotoxicity and apoptotic assays, and qPCR and Western Blot analyses, have been carried out to assess the potency and to characterize the binding mode of the newly identified lead compound. The absence of toxicity towards normal cells, together with the small molecular weight (≅ 500), the water solubility, the ease of functionalization, and the selectivity profile are promising and desirable features to develop G-quadruplex binders as safe and effective anticancer agents.

Introduction

Since the early observations that guanine-rich nucleic acids can adopt highly ordered secondary structures,[1] biological relevance and therapeutic value of non-canonical DNA secondary structures have been both very active and attractive fields in the drug discovery arena. Among them, G-quadruplexes (G4s) stand for the most investigated ones and have gained the status of clinically validated targets in oncology, with Quarfloxin as first-in-class compound reaching Phase II clinical trials,[2] but failing to proceed for bioavailability issues. The G4s are a heterogeneous class of structural topologies composed of hydrogen-bonding arrangements of four guanine bases, namely the G-tetrads, which are the G4s' core-motif, or, quoting S. Neidle "the cement that holds G-quadruplex structures together". [3] In the late 80' pioneering works by Henderson[4] and Sundquist and Klug,[5] sparked an interest in the involvement of G4s in telomeric processes[6-9] and in potential therapeutic applications. A few years later, cardinal work of the Hurley and Neidle labs provided the first G4 ligands that effectively inhibited telomerase and induced cancer cell death by restoring the activation of the apoptotic pathways.[10-12]

G4-forming motifs have also been identified in oncogene promoter regions,[13-15] bringing to light the therapeutic potential for targeted gene regulation at the transcriptional level.[16] The most studied oncogene promoter G4s include *c-MYC*,[17] *BCL-2*,[18-19] *h-RAS*,[20] *k-RAS*,[21] and *c-KIT*.[22-23] Soon after the leading works addressing the identification and the biological relevance of gene promoters' G4 binders, it became apparent that the indirect targeting of a protein overexpressed in tumor cells, by the direct targeting of its coding gene could have some key advantages compared to proteins,[24] such as fewer copies of target, lower probability of resistance and mutations, and possibility to target genes even when their products proved to be undruggable as in the case of *c-MYC*. Nevertheless, important challenges are associated with the development of potent and selective G4 binders, with the poor availability of promoter G4s' structural information being one the most limiting issues. Albeit selective ligands rationale design is most desirable,[25] and some successful applications of computational techniques have been reported, different G4s' selective ligands also arose from the application of fragment-based screening,[26] and dynamic combinatorial libraries.[27-29] Thanks to these

approaches, a good number of ligands with different selectivity profiles have been reported so far, the most being *c-MYC* G4 selective binders.[30-36] Other reported chemotypes able to selectively bind gene promoter G4s over duplex and sometimes also over telomeric G4s, include, but are not limited to, indolo[3,2-*b*]quinolines (human telomeric, *c-KIT2* and *Hsp90A* G4s),[37] indenopyrimidine derivatives (*c-KIT* and *c-MYC* G4s),[38] indolylmethyleneindanone scaffolds (*c-KIT* and *c-MYC* G4s),[39] piperidinyl-amines (*c-KIT* and *c-MYC* G4s),[40] synthetic derivatives of two natural compounds, berberine and palmatine (*c-KIT* and *c-MYC* G4s),[41] and furopyridazinones (*BCL-2* G4),[42] tri-substituted isoalloxazines (*c-KIT1* and *c-KIT2* G4s),[43] and bis-indole carboxamides (*c-KIT2* and *c-MYC* G4s).[44] These important findings demonstrated that, in particular for the end-stacker ligands, selectivity for the G4s over the duplex DNA, could be achieved increasing both the number of side chains substituents and ligand size, so that π-π interactions with the larger surface area of a terminal G-tetrad could be maximized. But, clearly, these structural requirements – higher molecular weights and increased cationic charges – lower the drug-likeness of the G4 ligands. In the search for new drug-like molecular entities able to selectively target gene promoter G4s, here we propose a bio-inspired approach focusing on the use of nucleobases as chemical platform to get three different new classes of compounds: 6-alkyl-3-(alkylamino)-2arylimidazo[1,2-*c*]pyrimidin-5(6*H*)-ones (**1**), 1-alkyl-8-(alkylamino)-7-aryl-1*H*-imidazo[2,1-*b*]purin-4(5*H*)-ones (**2**), and *N*-alkyl-3-alkyl-8-aryl-3*H*-imidazo[2,1-*i*]purin-7-amines (**3**) when cytosine, guanine, and adenine were used as starting materials, respectively (Figure 1).

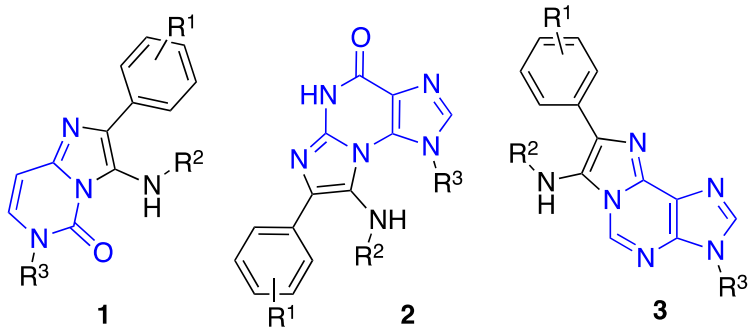

Figure 1. Bio-inspired key scaffolds **1**, **2**, and **3** (nucleobases' structural cores are highlighted in blue).

The underlying concept aims to create libraries of new molecular scaffolds exploiting the chemical nature of nucleobases, which are intrinsically able to accept and donate hydrogen bonds and to make efficient π-stacking interactions with each other and hence potentially, with the target nucleic acids sequences. We speculated that harnessing the structural features of the nucleobases would create a library with desirable G4s' binding properties. Moreover, the presence of a high nitrogen/carbon *ratio* in the imidazo[2,1-*i*]purin-7-amine molecular frame (which means, potentially, formation of more hydrogen bonds), and the possibility to functionalize this scaffold with a range of cationic side chains, would offer the possibility to fine tune selectivity towards different G4 topologies.

Results and Discussion

Selection of the lead compound. In order to test our hypothesis, we synthesized compounds **4**-**6** (Figure 2), representative of the use of three different nucleobases as synthons (cytosine, guanine, and adenine, respectively), and functionalized with a 2-ethylmorpholino moiety in order to add a basic amino group, which, in its protonated form, could provide an ionic interaction with the negatively charged DNA phosphates. Compounds **4**-**6** were hence preliminarily screened for their ability to stabilize G4s in a circular dichroism (CD) melting assay.[45]

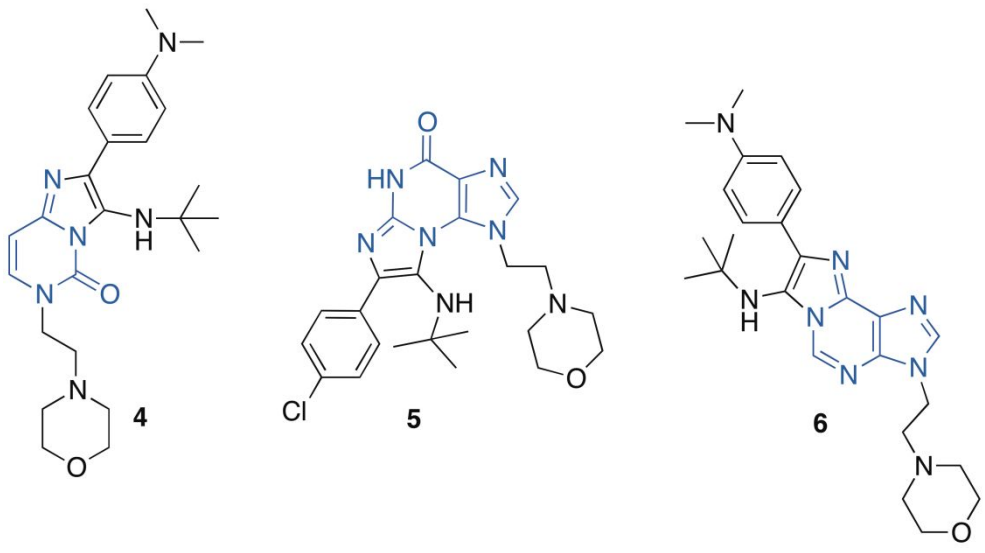

Figure 2. Bio-inspired potential leads **4**, **5**, and **6**.

In particular, three G4 -forming sequences from the oncogene promoter regions of *BCL-2* (*BCL2*-G4), *c-KIT* (*c-KIT1*-G4) and *c-MYC* (*c-MYC*-G4), as well as a 23-mer truncation of human telomeric DNA sequence (*Tel23*-G4) were used in these experiments. Moreover, a 20-mer hairpin-duplex-forming sequence (*Hairpin 20-mer*) was also used in order to evaluate the G4s' over duplex selectivity of the compounds.

The overall topology adopted by each investigated DNA sequence was first verified by CD measurements (Supporting Information, Figure S1). *c-KIT1* and *c-MYC* sequences adopted parallel G4 conformations, showing the characteristic positive band at 262 nm and negative band at 240 nm in their CD spectra. The presence of an additional band at 290 nm in the CD spectrum of *BCL-2* clearly indicates the formation of a mixed parallel/antiparallel conformation. On the other hand, *Tel23* sequence showed a CD spectrum having two positive bands at 290 and 270 nm and a weak negative band at 240 nm, consistent with the formation of a hybrid [3+1] G4 folding topology. As mentioned above, we also took into consideration a hairpin-duplex-forming sequence showing a positive band at 270 nm and a negative one at around 230 nm in the CD spectrum, which are characteristic values of duplex formation. Next, CD studies were performed to explore the potential of **4**-**6** to alter the native folding topology of the investigated G4s. Upon addition of an excess of ligands (10 molar equivalents relative to the DNA), no relevant variations of DNA chiroptical signals were observed, suggesting an overall preservation of the DNA structure in the presence of **4**-**6** (Supporting Information, Figure S1). Then, the DNA stabilizing properties of compounds **4**-**6** were evaluated by CD-melting experiments measuring the ligand-induced change in the melting temperature (ΔT_m) either of G4 and duplex structures (Supporting Information, Figure S2). Results of these experiments clearly revealed that **4** and **5** did not increase significantly the stability of any G4 as well as of duplex DNA (Figure 3). On the other hand, compound **6** turned out to be able to induce a noticeable increase of the melting temperatures of the three gene promoter G4s (*BCL2* G4: ΔT_m = 9.2 ±0.5 °C; *c-MYC* G4: ΔT_m = 7.2 ±0.5 °C; *c-KIT1* G4: ΔT_m = 5.2 ±0.5 °C), suggesting a good affinity of **6** for the parallel G4 conformation adopted by them. Conversely compound **6** did not increase significantly the thermal stabilities of the antiparallel telomeric G4 (*Tel23* G4: ΔT_m = 2.4 ±0.5 °C), as well as of the hairpin-duplex DNA (*Hairpin 20-mer*: ΔT_m = 1.9 ±0.5 °C) giving a glimpse of its G4's over duplex selectivity, and also providing a first evidence of its ability to discriminate

among different G4 topologies. In light of these preliminary results, compound **6** was selected as our lead compound and a library of 16 analogues was synthesized and tested in both biophysical and biological assays.

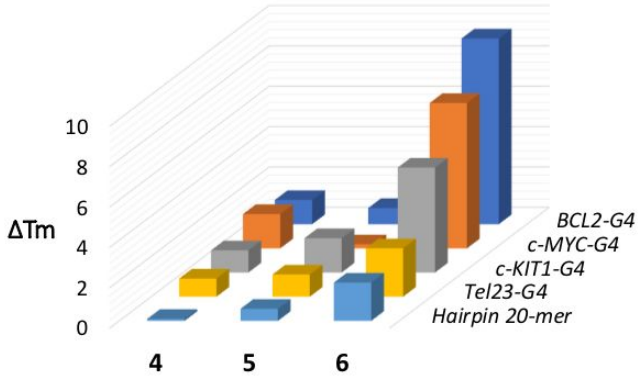

Figure 3. Variation of the melting temperature (ΔT_m) of different G4-forming sequences and of a hairpin-duplex-forming sequence induced by compounds **4-6**. Errors are ±0.5 °C.

Synthesis of the focused library. Compounds **4-21** were synthesized in two steps, namely a Groebke-Blackburn-Bienaymé 3-component reaction (GBB-3CR)[46] and a subsequent S_N2 with 2- and 3-aminoalkyl halides (Scheme 1). The GBB-3CR is a multicomponent reaction involving a 2-amino-aza-heterocycle, a benzaldehyde and an isocyanide. Herein we used nucleobases[47] such as cytosine, guanine and adenine as starting materials, six different substituted benzaldehydes, and *tert*-butylisocyanide. By performing the GBB-3CR in DMSO as the solvent, using $ZrCl_4$ as Lewis acid catalyst, at 70 °C overnight, compounds **A-G** (GBB-3CR adducts) were obtained in 11–50 % yields. Their subsequent alkylation was performed in DMF, using Cs_2CO_3 as base, at 100 °C, overnight, to give compounds **4-21** with yields ranging from 22 to 84%. While variously substituted aldehydes and different 2- and 3-aminoalkyl halides have been selected as starting materials, *tert*-butyl isocyanide was chosen as a highly nucleophilic component of the GBB-3CR.

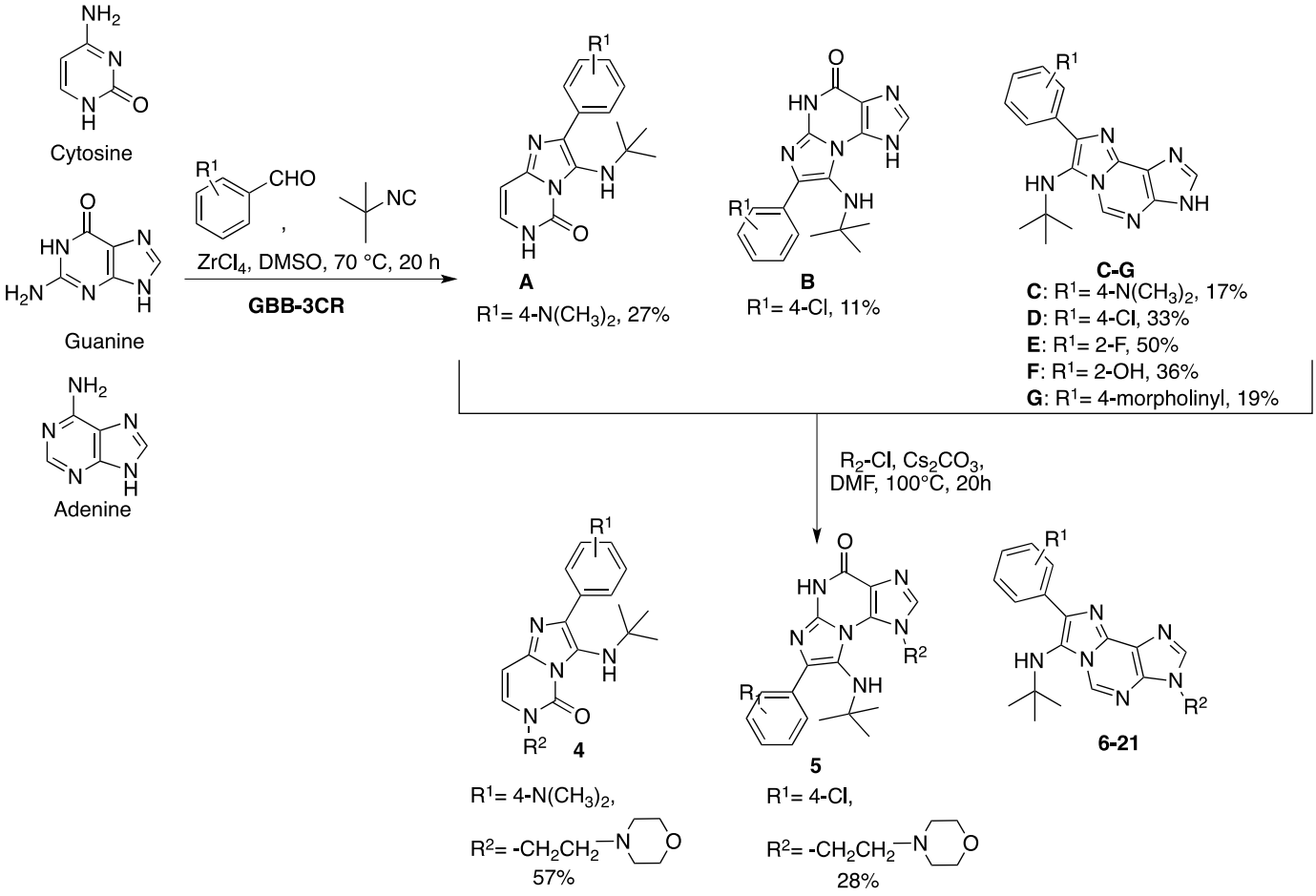
Cytosine
Guanine
Adenine
CHO
NC
ZrCl4, DMSO, 70 °C, 20 h
GBB-3CR
A
R1= 4-N(CH3)2, 27%
B
R1= 4-Cl, 11%
C-G
C: R1= 4-N(CH3)2, 17%
D: R1= 4-Cl, 33%
E: R1= 2-F, 50%
F: R1= 2-OH, 36%
G: R1= 4-morpholinyl, 19%
R2-Cl, Cs2CO3,
DMF, 100°C, 20h
4
R1= 4-N(CH3)2,
R2= -CH2CH2-N O
57%
5
R1= 4-Cl,
R2= -CH2CH2-N O
28%
6-21

Compd	R^1	R^2	Yield
6	4-$N(CH_3)_2$	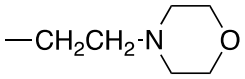	56%
7	4-$N(CH_3)_2$	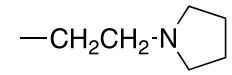	63%
8	4-$N(CH_3)_2$	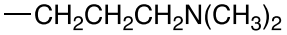	84%
9	4-$N(CH_3)_2$	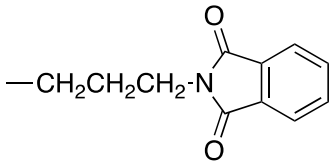	56%
10	4-Cl	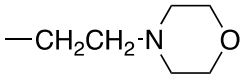	37%
11	4-Cl	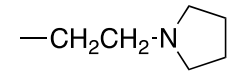	63%
12	4-Cl	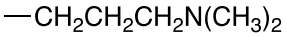	59%
13	2-F	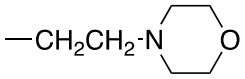	42%
14	2-F	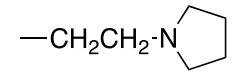	69%
15	2-F	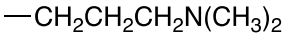	47%
16	2-OR^2	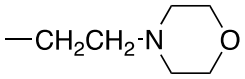	31%
17	2-OR^2	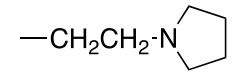	35%
18	2-OR^2	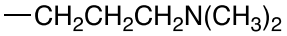	22%
19	4-morpholine	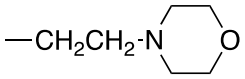	68%
20	4-morpholine	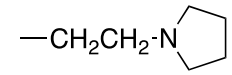	67%
21	4-morpholine	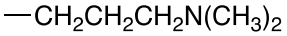	48%

Scheme 1. Synthesis of compounds **4-21**.

According to Scheme 2, compound **9** was deprotected with hydrazine hydrate, to give the free amino group in compound **22**, and the latter was further derivatized with *S*-ethylthiopseudourea in order to get the guanidino functional group (**23**).[48]

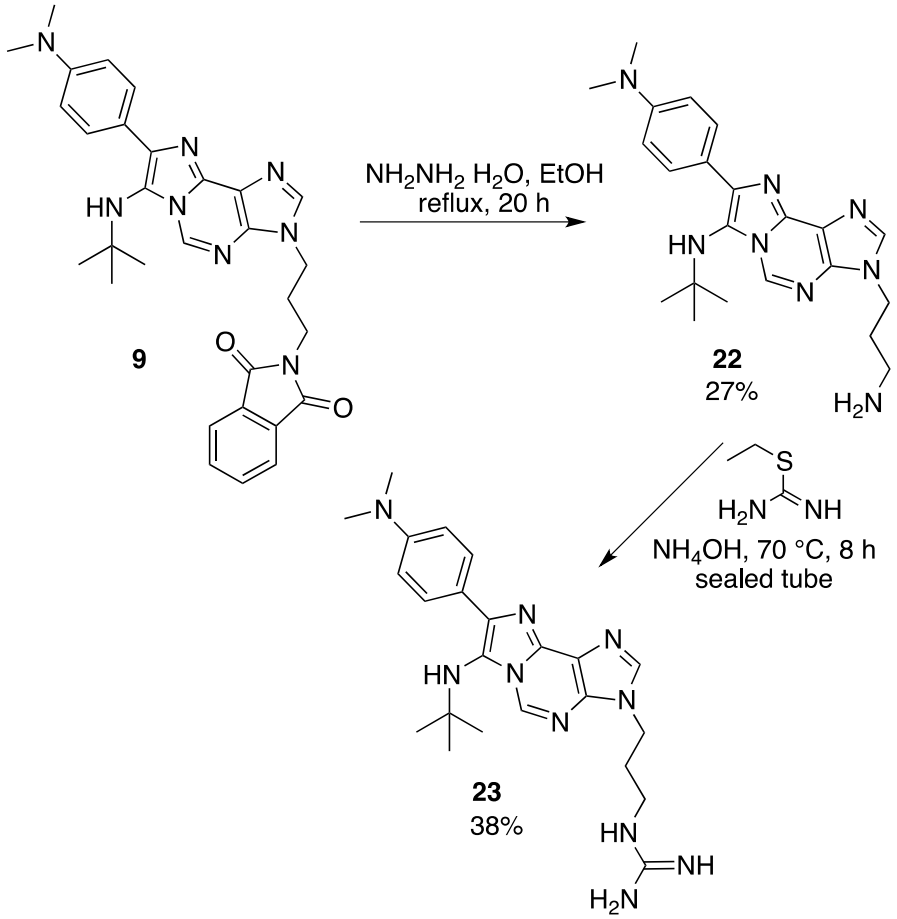

Scheme 2. Synthesis of compounds **22**-**23**.

Circular dichroism studies. With the aim of evaluating the interaction of compounds **7**-**8**, **10**-**23** with G4 structures and their selectivity for G4 over duplex DNA, CD melting experiments were performed using the same DNA sequences already used for testing compounds **4**-**6**. Results of such experiments are reported in Table 1 (and Supporting Information, Figures S3-S4).

Starting from lead compound **6**, when the ethylmorpholino chain (-R_2, Scheme 1) was substituted with ethylpyrrolidine (**7**) or *N*,*N*-dimethylpropylamine (**8**), an increase of thermal stabilization of G4s was observed even at the expenses of their selectivity. In fact, compounds **7** and **8** showed to be not able to discriminate G4 over duplex DNA (Table 1). On the other hand, the functionalization of the alkyl chain with a primary amino group (**22**) or a guanidino unit (**23**) led to a dramatic drop in potency. In addition, while the replacement of the 4-*N*,*N*-dimethylamino group of the aryl ring of lead compound **6** (R_1, Scheme 1) with a halogen atom as a 4-Cl (**10**) led to a lower T_m variation , the concomitant presence of aminopyrrolidine (**11**)

and *N*,*N*-dimethylpropylamine (**12**), induced an increased G4 stabilization and a better selectivity towards *BCL2* G4 and c-*MYC* G4 over the other investigated G4s and duplex DNA (Table 1).

Table 1. Melting temperature variations of G4 and hairpin-duplex DNAs upon addition of 10 molar equivalents of compounds **7**-**8** and **10**-**23** measured by CD melting experiments.[a]

Compound	*BCL2*-G4	*c-MYC*-G4	*c-KIT1*-G4	*Tel23*-G4	*Hairpin-20-mer*
7	+ 13.4	+ 19.5	+ 7.3	+ 4.8	+ 7.5
8	+ 16.9	> + 25.0[b]	+ 11.9	+ 7.2	N.D.[c]
10	+ 2.1	+ 1.6	+ 1.1	+ 0.3	- 0.5
11	+ 4.5	+ 6.4	+ 2.3	+ 2.3	+ 1.9
12	+6.7	+ 12.8	+ 2.8	+ 2.4	- 0.5
13	+ 2.6	+ 1.9	+ 1.0	+ 0.7	+ 0.5
14	+ 5.0	+ 5.8	+ 2.1	+ 1.1	+ 0.3
15	+ 8.2	+ 11.5	+ 2.6	+ 1.2	+ 0.2
16	+ 1.9	+ 1.9	+ 0.8	+ 0.1	+ 1.2
17	+ 7.1	+ 8.4	+ 4.5	+ 4.9	+ 2.2
18	+ 7.8	> + 25.0[b]	+ 4.5	+ 5.7	+ 3.5
19	+ 4.9	+ 2.1	+ 1.9	+ 1.0	+ 1.5
20	+ 9.1	+ 8.7	+ 2.9	+ 2.2	+ 6.0
21	+ 10.1	+ 9.5	+ 5.1	+ 3.8	+ 9.7
22	+ 1.7	+ 1.1	+ 1.4	- 0.1	+ 0.5
23	+ 2.8	+ 2.5	+ 2.1	+ 0.6	+ 0.2

[a]ΔT_m represents the difference in melting temperature [$\Delta T_m = T_m$ (DNA + 10 ligand equivalents) - T_m (DNA)]. The T_m values of DNAs alone are: *BCL2*= 61.5 ± 0.5 °C; *c-MYC* = 78.4 ± 0.5 °C *c-KIT1*= 54.7 ± 0.5 °C; *Tel23*= 54.5 ± 0.5 °C; *Hairpin-20-mer* = 62.3 ± 0.5 °C. [b]These compounds increase significantly the thermal stability of the G4; however ΔT_m values are not accurately determinable (T_m >100 °C). [c]ΔT_m value is not determinable due to the presence of multiple transitions in the melting curve.

When the halogen atom on the aryl ring was a 2-F group as in compounds **13**-**15**, the ethylmorpholino chain (**13**) provided weak interactions, while ethylpyrrolidine (**14**) and *N*,*N*-dimethylpropylamine (**15**) were able to induce a higher thermal stabilization of both *BCL2* and *c-MYC* G4s, while showing poor binding to *c-KIT1* and *Tel23* G4s, and absolutely no binding to the duplex DNA (Table 1). We also investigated the effect of a double aminoalkyl chain as in compounds **16**-**18**, with the aim to check if the presence of two cationic charges, as present in many G4 binding ligands, could improve affinity of the lead compound **6**. When the

scaffold was decorated with two ethylmorpholino chains (**16**), a very weak stabilization of both G4s and duplex DNA structures was observed, while unfortunately the ethylpyrrolidine (**17**) and *N*,*N*-dimethylpropylamine (**18**) chains induced an indiscriminate binding to both G4s and duplex DNA (Table 1). Finally, compounds **19**-**21** showed that the effect of a bulkier substituent on the aryl ring such as the 4-morpholino group, was detrimental, since it led to a loss of selectivity for G4s over duplex DNA (Table 1). In view of the above results, compounds **12**, **15**, and **19** were selected as the best performing ones due to their high selectivity over duplex DNA and preference for the *BCL2* and *c-MYC* G4 architectures over others. Therefore, a more in-depth biological and biophysical characterization of the interaction properties of **12**, **15**, and **19** with *BCL2* and *c-MYC* G4s was carried out.

Evaluation of the cytotoxic activity of the selected compounds. The simultaneous targeting of two non-canonical DNA secondary structures, in particular *c-MYC* G4 and *BCL2* i-Motif, has been shown as a synergistic and valid approach to lower mRNA levels of anti-apoptotic proteins and overcome aberrant pathways in cancer cells.[49] Encouraged by these previous findings, and with the aim to evaluate the cellular effects of compounds **12**, **15**, and **19** upon interaction with the gene promoter *BCL2* and *c-MYC* G4s, further biological studies were performed. Within the framework of preliminary screening *in vitro,* the bioactivity profile of the compounds was first evaluated on the human leukemia cell line Jurkat, where Bcl2 is known to play a critical role in the regulation of cell survival.[50] To this aim, at the outset the cells were incubated in the presence of the ligands for 48 h at concentrations ranging from 5 to 50 μM. The results depicted in Figure 4A - here reported grouping data into a single indicator defined as "cell survival index" combining mitochondrial metabolic activity and cell counting - show a remarkable dose-dependent cytotoxic activity for compound **12** on Jurkat cells, with a cell survival index that drops below 25% to the highest tested concentrations. In the same experimental condition, the bioactivities related to compounds **15** and **19** were yet significant but less effective in blocking cell growth and proliferation. Indeed, compound **15** induced a decrease of cell survival of about 60% at 50 μM, while compound **19** showed only a weak cytotoxic activity. Therefore, we next investigated more thoroughly the bioactivity profile of compound **12** by using a selected

panel of human cancer cells of different histological origin. Concentration-effect curves in Figure 4B suggest compound **12** as basically inactive on human breast adenocarcinoma cells (MCF-7 cell line), as well as on colorectal and melanoma cells (HCT-116 and A375, respectively). This selectivity of action for compound **12** is highlighted by the calculation of IC_{50} values (data reported in Figure 4D), indicating a marked antiproliferative effect on Jurkat cells with an IC_{50} in the low micromolar range (17 μM) and no interference with the growth of the other tumor cells tested - an interesting outcome for further future development of this compound. Accordingly, under the same conditions, evidences emerging from bioscreen on non-malignant cells (Figure 4C), as human keratinocytes (HaCaT) and human dermal fibroblast (HDF), only show a weak cytotoxicity at concentrations *in vitro* higher than 50 μM.

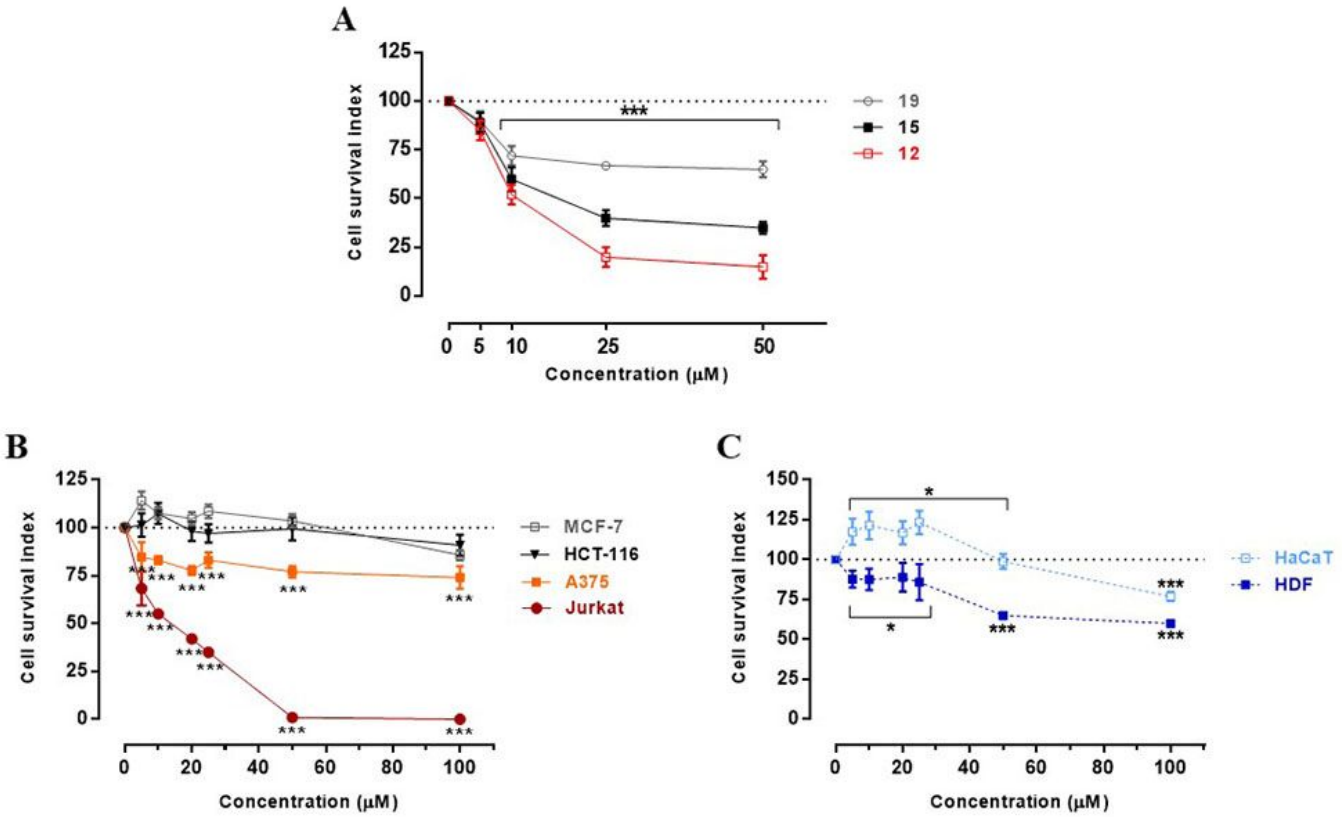

D

IC_{50} (μM)	MCF-7	HCT-116	A375	JURKAT	HaCaT	HDF
12	> 100	> 100	> 100	17 ± 2	> 100	80 ± 20

Figure 4. (**A**) Cell survival index, evaluated by the MTT assay and the analysis of the live/dead cell ratio, for Jurkat cells following 48 h of incubation with the indicated concentration (5, 10, 25 and 50 μM) of

compounds **12**, **15** and **19**. Data are expressed as percentage of untreated cells and are reported as mean of 3 independent experiments ± SEM (n = 18). ***p<0.001 *vs.* control (untreated cells). (**B**) Cell survival index for human cancer MCF-7, HCT-116, A375 and Jurkat cells, and (**C**) for human non-cancer HaCaT and HDF cells, after treatments for 48 h with a range of concentrations (5 → 100 μM) of compound **12**, as indicated in the legends. *p<0.05 *vs.* control (untreated cells); ***p<0.001 *vs.* control (untreated cells). (**D**) IC_{50} values (μM) of compound **12** in the indicated cancer and non-cancer cell lines after 48 h of incubation *in vitro*. IC_{50} values are reported as mean ± SEM (n=18).

To determine whether **12**, **15**, and **19** were able to induce apoptotic cell death, Jurkat cells were treated with the compounds for 48 h, and the apoptosis analysis was performed with annexin V-FITC/PI double staining by flow cytometry analysis.[51] Consistent with bioscreen *in vitro*, the assay showed that the entire population of cells (99%) treated with compound **12** was in the late apoptotic state (Figure 5B), while for compound **15** the 68% of cells were found to be in advanced apoptosis and 13% in early apoptosis (Figure 5C) with respect to the control (Figure 5A). In contrast, when cells were treated with compound **19**, only slight percentages, 9 and 8%, were found in the advanced and in the early apoptotic stage, respectively (Figure 5D).

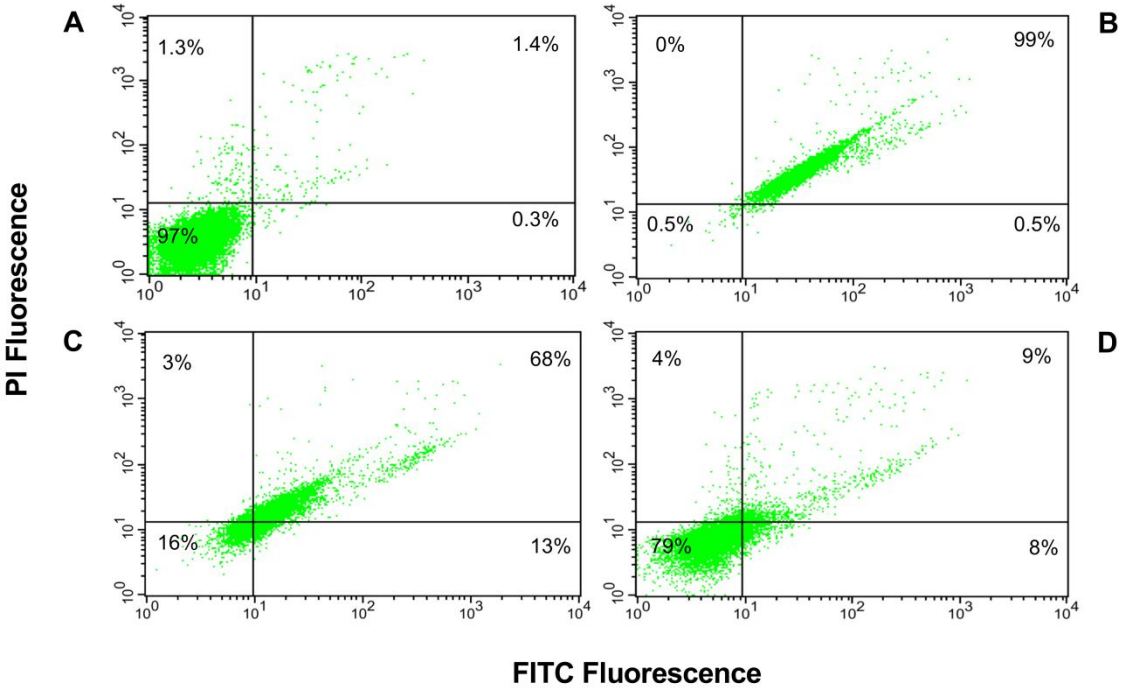

Figure 5. Apoptosis analysis with annexin V-FITC/PI double staining on Jurkat cells. Jurkat were treated with 25 μM molecules for 48 h. (A) Control (vehicle treated cells); (B) **12**; (C) **15**; (D) **19** treated cells. Lower left quadrant: viable cells; upper left: necrotic cells; upper right: advanced apoptotic cells, low right: early apoptotic cells. This picture is representative of two independent experiments.

Downregulation of Bcl2 and c-Myc mRNAs, and effects on protein expression. To determine the effect of **12**, **15**, and **19** on *BCL2* and *c-MYC* gene transcription, quantitative analysis of mRNA was carried out by means of real-time qPCR analyses (Figure S5). Upon treatment of Jurkat cells with 25 μM of selected compounds for 24 h, the cells were lysed to obtain the total RNA. qPCR analysis showed a reduction of about 66 and 56 % of c-*MYC* expression when cells were treated with compounds **12** and **15**, respectively. Differently, **19** induced a decrease of the expression level of *c-MYC* of only 27%. In the same manner, *BCL2* expression resulted to be inhibited of 67 and 43% after **12** and **15** treatments, respectively. In parallel, to confirm that the observed decrease in mRNA levels effectively leads to a decrease in Bcl-2 and *c*-Myc protein content, Western blot analysis was performed on cellular extracts by using anti-Bcl-2 and anti-*c*-Myc antibodies (Figure 6). Accordingly, immunoblot experiments revealed compound **12** able to decrease of about 50 and 40% *c*-Myc and Bcl-2 levels, respectively. In line with qPCR analysis, compounds **15** and **19** were less effective but still able to significantly decrease *c*-Myc and Bcl-2 protein content under the same experimental conditions.

Based on the results obtained from cytotoxicity assays, on the ability to induce apoptotic death in Jurkat cells, to down-regulate Bcl2 and *c*-Myc mRNAs, as well as to decrease both *c*-Myc and Bcl-2 protein expression, compound **12** was selected as the most promising of the library and engaged in further biophysical studies in order to better characterize its activity towards *BCL2* and *c-MYC* G4s.

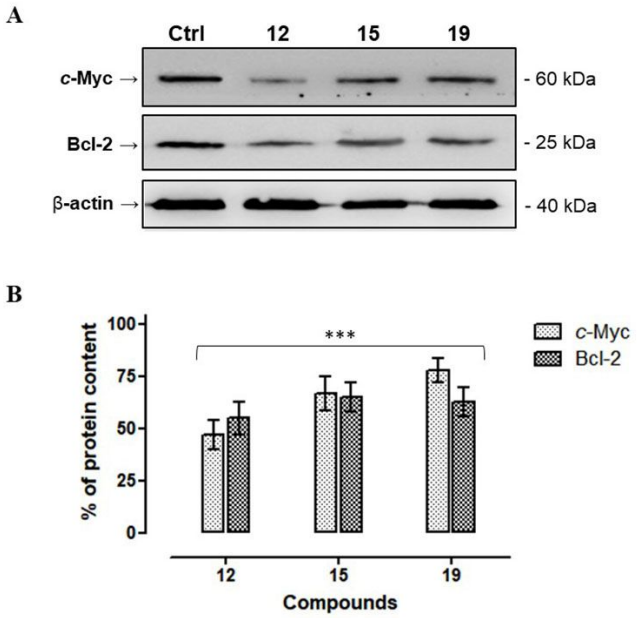

Figure 6. (A) Western blot analysis showing the effects of compounds **12**, **15** and **19** in Jurkat cells on the expression of *c*-Myc and Bcl-2 proteins following 24 h of incubation at 25 μM. The shown blots are representative of three independent experiments and are cropped from different parts of the same gel, as explicit by using clear delineation with dividing lines and white space. **(B)** After chemiluminescence, the bands resulting from cell extracts were quantified by densitometric analysis and plotted in bar graphs as percentage of controls (100% of protein content), as indicated. Shown are the average ± SEM values of three independent experiments. The anti-β-actin antibody was used to standardize the amount of proteins in each lane. *** $p<0.001$ *vs.* control untreated cells.

Microscale Thermophoresis experiments. The binding affinity of **12** for *BCL2* and *c-MYC* G4s was measured by means of microscale thermophoresis (MST).[52] MST is a rapid and easy methodology to quantify interactions between small molecules and nucleic acids in solution.[53] In MST experiment, one of the interacting partners must be fluorescent (either intrinsically fluorescent or a fluorophore is conjugated to a non-fluorescent target). The binding of a ligand to the investigated molecule changes the thermophoretic behavior of the target. This effect can be used to evaluate equilibrium constants, such as the dissociation constant K_d. To this purpose, serial dilutions of **12** were prepared, mixed with a constant concentration of Cy5-labeled oligonucleotides (*BCL2* and *c-MYC*), loaded into capillaries and analyzed by MST. Experiments

were run by using 5% final DMSO, in order to better solubilize the ligand. The results of these experiments (Figure 7A, B) showed that compound **12** was able to bind both *BCL2* and *c-MYC* G4s. with estimated K_d values in the micromolar range [K_d= 26 (±7) μM and 60 (±20) μM for *c-MYC* and *BCL2,* respectively]. Control experiments were also performed using *c-KIT1*, telomeric and hairpin 20-mer sequences. Results of such experiments (Figure S6) clearly show no interaction of compound **12** with both telomeric and hairpin 20-mer DNAs. On the other hand, compound **12** turned out to be able to interact also with *c-KIT1* G4 (estimated K_d= 51 (±10) μM, Figure S6C), thus confirming a ligand binding specificity towards parallel G4s.

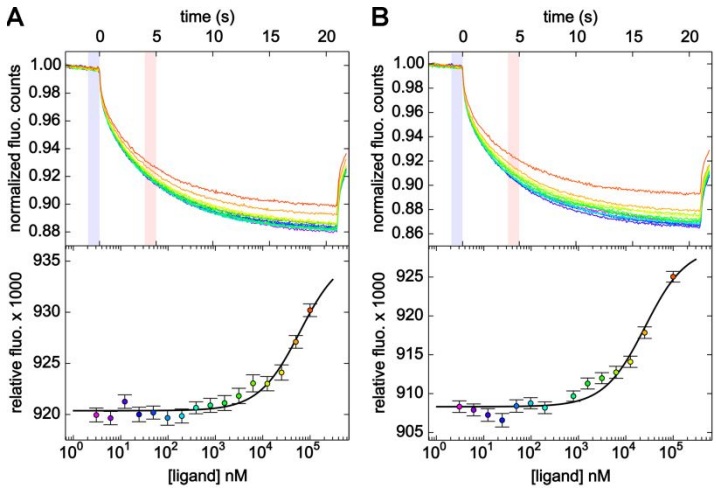

Figure 7. MST measurements on the interaction of compound **12** with (A) *BCL2* and (B) *c-MYC* G4s. (Top) Time traces recorded by incubating increasing concentrations of **12** with the labeled G4s and (bottom) the corresponding binding curves.

NMR spectroscopy titration experiments. In order to get information about the binding mode of compound **12** to *BCL2* G4 and *c-MYC* G4, ^{1}H-NMR titration experiments were performed.[45] According to the literature, the *BCL2* and *c-MYC* sequences form, under the experimental conditions used, a single G4 conformation characterized by 12 well-resolved imino proton peaks, corresponding to the 12 guanines involved in the three G-tetrad planes (Figure 8). [19, 54] The investigated oligonucleotides were then titrated with **12** up to a 5:1 ligand/G4 ratio. In both cases, upon addition of increasing amounts of ligand to the G4 solutions, gradual chemical shift changes for some DNA proton signals were observed. However, the imino and the aromatic

regions of the spectra were affected with a different extent for the two G4s. Some signals of the compound were also detected in the spectra. These peaks only grew in intensity, without showing any significant change in chemical shift values by increasing ligand concentration, clearly suggesting a rapid binding process on the NMR timescale. To probe the structural origin of the interaction between **12** and the two G4 structures, the chemical shift variations (Δδ) of *BCL2* G4 and *c-MYC* G4 were calculated (Supporting Information, Table S1).

As far as *BCL2* G4 is concerned, the largest perturbations were observed for the imino protons belonging the 3' G-tetrad (G3, G7 and G19), as well as for some of those of the middle G-tetrad (G2 and G8). Conversely, the imino protons of the 5' G-tetrad (G1−G9−G17−G21) were not affected at all. Furthermore, ligand interaction with *BCL2* G4 (Figure 8A) also significantly affected the aromatic proton of C4 located in the lateral loop adjacent to the 3'-tetrad, as well as the aromatic protons of G3 and G7.

On the other hand, upon addition of compound **12** to the *c-MYC* G4 solution the imino signals belonging to the G-tetrad on the 5'-side (G7−G11−G16−G20) as well as of those belonging to the 3'-face (G9−G13−G18−G22) were strongly affected, while the remaining imino protons of the middle tetrad (G8−G12−G17−G21) turned out to be slightly less affected (Figure 8B). Concerning the 5'-face of *c-MYC* G4, it is more accessible for ligand stacking than 3' one and the only 5'-flanking residue mainly affected by the binding turned out to be the A6. At the 3'-side, the G4 NMR structure reveals that A25 folds back to form a base pair with T23, thus covering the external 3' G-tetrad, along with A24 that stacks on the T23:A25 base pair. However, upon addition of **12**, the aromatic protons of T23, A24, and A25 show a strong perturbation, thus suggesting that such bases were not able to prevent the binding and that the ligand could stack on the 3' G-tetrad displacing the architecture of 3'-flanking bases.

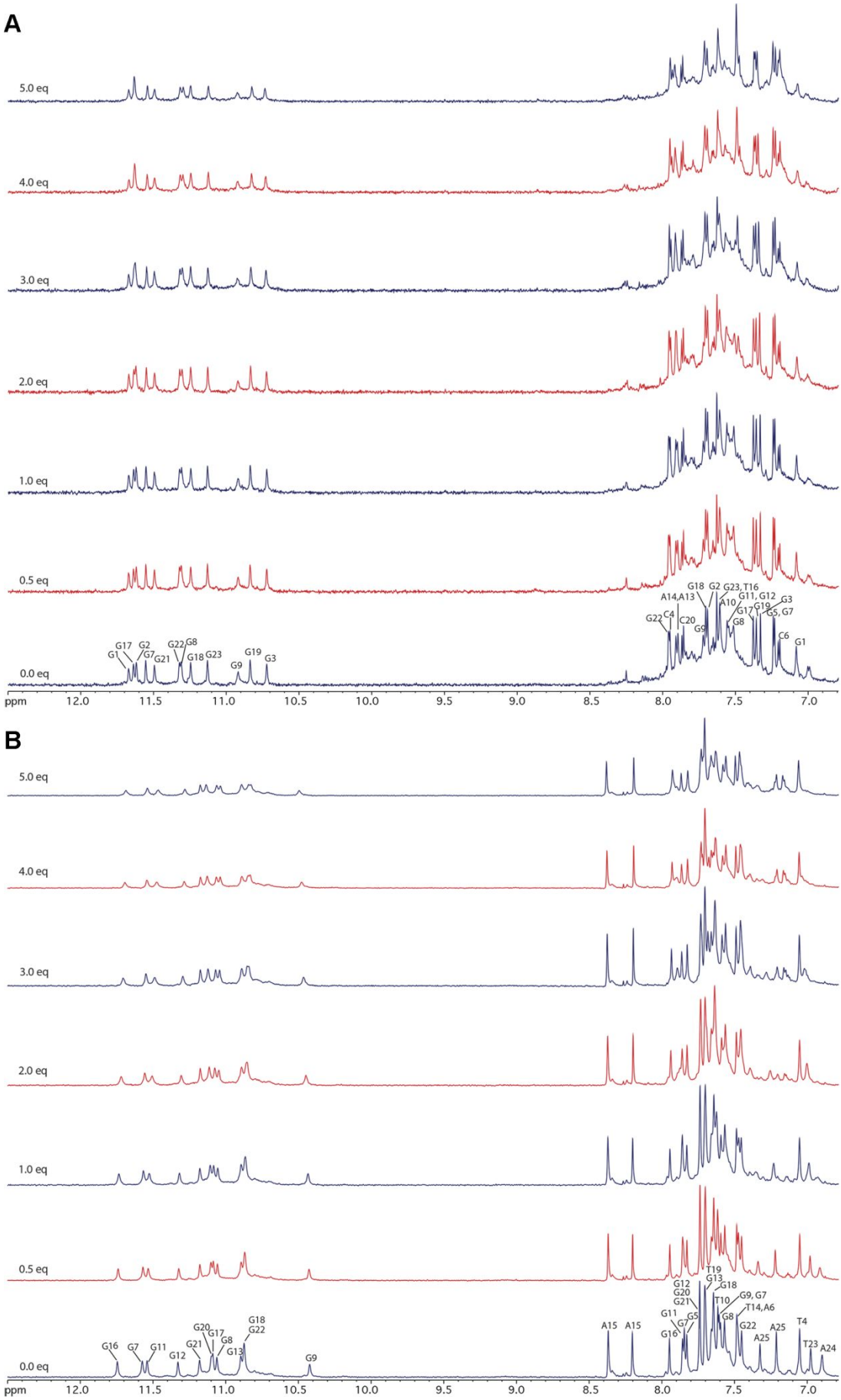

Figure 8. ^{1}H NMR spectra of (A) *BCL2* and (B) *c-MYC* G4s titrated with compound **12**. The ligand equivalents are shown on the left of the spectra.

Computational docking studies. To visualize the potential binding mode of **12** we performed a docking study. Regarding the *c-MYC* G4 sequence, we selected the three NMR models with the following PDB codes: 1XAV, 2L7V, and 5W77. The first is formed by 20 conformations of a monomeric parallel-stranded G4,[52] the second is formed by 10 different conformations[55] and is complexed with a quinoline ligand, while the latter is formed by 15 different conformations[56] and is in complex with a benzofuran ligand. As concerns the *BCL2* G4 sequence, an NMR structure (PDB code: 2F8U) has been taken into account.[19] This structure is a monomer characterized by 10 different conformations. All the above-described experimental structures were prepared and refined. Then, we performed a molecular docking study, using software FRED[57-58] to identify a potential binding mode of **12** against 45 and 15 conformations of *c-MYC* G4 and *BCL2* G4 respectively (Supporting Information, Tables S2-S3). Based on the interaction energy predicted by FRED, the best complex of compound **12** and *c-MYC* and *BCL2* G4S were selected.

In the complexes with *c-MYC* G4, compounds **12** appeared to prefer the 5'-end position (Figure 9A, C) by π-π stacking interactions with G5 and G16, while NH group is involved in a hydrogen bond interaction with G11. Moreover, a putative hydrogen bond between a protonated tertiary amine and G7 could be present. Compound **12** showed a very similar binding orientation compared to a quindoline structure already crystalized with *c-MYC* G4 (PDB code: 2L7V). Docking results indicate a preference for 5'-side of compound **12**, this could be a consequence of the conformation of T23:A25 in the considered *c-MYC* G4 structures that prevent **12** to bind near the 3' G-tetrad. This result is in contrast with the NMR titration spectra showing that compound **12** is able to displace the 3'-flanking bases and stack also on the 3' G-tetrad. As regards the complexes of *BCL2* G4 (Figure 9B, D), compound **12** assumed a different binding mode. In accordance with spectral NMR data showing the largest perturbations for the imino protons belonging the 3' G-tetrad (G3, G7 and G19), and the middle G-tetrad (G2 and G8), the docking results indicate that **12** is located near C4, G7 and G8, but with an orientation that does not allow π-π stacking interactions, while NH group gives hydrogen bond interactions with the phosphate link between G8 and G9 and also a putative hydrogen bond between a protonated tertiary amine and phosphate group of G7 could be present. From both NMR and molecular docking studies it is possible to elucidate the following structure-activity relationship:

in the interaction with *c*-MYC G4, the heteroaromatic imidazo[2,1-*i*]purinic scaffold forms π-stacking interactions with guanines 5 and 16 at the 5'-end, and, as evident from NMR spectra, with the 3'-flanking bases. Two hydrogen bonds are formed between the esocyclic NH of **12** and the guanine 11, and the protonated tertiary amine and the guanine 7, respectively. Hydrogen bonds between the NH group of **12** and the phosphate group linking guanines 8 and 9, and between the protonated tertiary amine and the guanine 7's phosphate group, represent key interactions in the binding to *BCL2* G4.

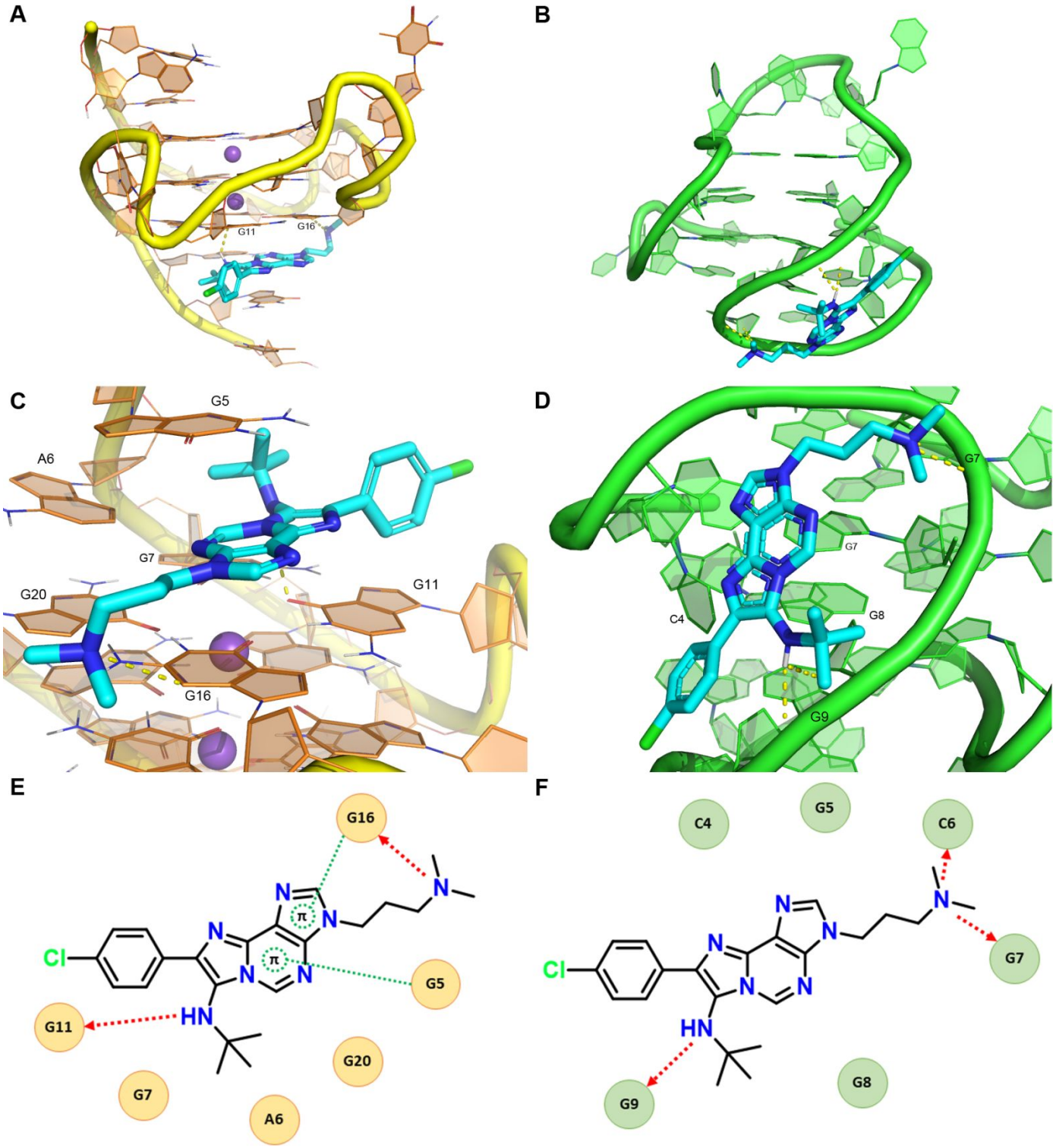

Figure 9. Best docked poses of 12 against *c-MYC* (A, C, E) and *BCL2* G4s (B, D, F) structures, respectively. The DNA of *c-MYC* (PDB id: 2L7V) and *BCL2* (PDB id: 2F8U) are shown as orange and green cartoons, respectively. The best 12 poses are represented as cyan carbon sticks. Coordinating K^+ ions are reported as violet spheres, while hydrogen bond interactions are indicated as dashed yellow lines. In the 2D depiction of

DNA-ligand interactions (E-F) *H*-bond and ππ stacking interactions are dashed red and green lines respectively.

Conclusions

Starting from three bio-inspired scaffolds (**4**, **5**, and **6**) synthesized through an atom-economical and convergent approach, namely a Groebke-Blackburn-Bienaymé three-component reaction, and a post-condensation S_N2, a new potential hit compound **6** has been selected by means of CD melting experiments performed on different G4 topologies. Accordingly, a focused library of 16 analogues has been synthesized and the binding efficiency towards different gene promoter G4s, as well as towards telomeric G4 and duplex DNA, has been evaluated. As a result, three new lead compounds, **12**, **15** and **19** have been selected as the best performing ones, both in terms of potency and selectivity towards *BCL2* and *c-MYC* G4s, over the other G4 topologies screened and a duplex model. In the context of preclinical studies *in vitro*, bioscreens on a selected panel of human cancer and non-cancer cells, as well as apoptotic induction assays, have been carried out to explore the bioactivity profile of the lead compounds, allowing us to select compound **12** as the most interesting one. Indeed, **12** exhibited a selective antiproliferative action towards Jurkat human T lymphoblastoid cells, without showing significant cytotoxicity towards normal cells such as skin-derived cells. Furthermore, a down-regulation at both mRNA and protein levels has been observed through qPCR and Western Blot analyses when cells were treated with the selected compounds. Even if these correlations do not rule out additional mechanisms contributing to the observed cellular responses, they are usually taken as a good validation of on-target (G4) effects. This feature, along with other important properties, such as small molecular weight (≅ 500), water-solubility (as hydrochloride salts), and ease of functionalization, account for the drug-likeness of the newly identified G4s' binders. Finally, in order to better characterize the *BCL2* and *c-MYC* G4s ligand binding profile, the dissociation constants K_d have been measured as in a low micromolar range via MST experiments, and the binding modes have been studied by both NMR titrations and computational docking calculations providing precious information for a future lead optimization. Altogether, the obtained data suggest that, albeit with a slight loss in potency if compared with less- or non-

selective G4 binders, the modulation of the selectivity towards different gene promoters'G4 could be feasible and biological relevant. In conclusion, a new class of bio-inspired drug-like dual selective *BCL2*/*c-MYC* G4 binders has been identified as new potential anticancer agents. Based on both the herein reported biophysical and biological data and the poor availability in literature of selective *BCL2*-G4 ligands, our lead **12** represents a promising advancement towards the pathway-specific targeting of cancer cell lines by means of gene promoters' G4 binders. Moreover, the reported approach, and the results obtained, provided evidence that capitalizing Nature's resources, such as nucleobases[59-60], as key structural elements could provide new molecular entities able to induce a fine-tuning of the selectivity towards different gene-promoter G4s and ergo safer anticancer drugs.

Experimental Section

Chemistry. General methods. Commercially available reagents and solvents were used without further purification. Dichloromethane was dried by distillation from P_2O_5 and stored over activated molecular sieves (4 Å). When necessary the reactions were performed in oven-dried glassware under a positive pressure of dry nitrogen. Melting points were determined in open glass capillaries and are uncorrected. All the compounds were characterized by IR. ^{1}H and ^{13}C APT NMR spectra were recorded on a 400 MHz. High-resolution ESI-MS spectra were performed on a Thermo LTQ Orbitrap XL mass spectrometer. The spectra were recorded by infusion into the ESI source using MeOH as the solvent. Chemical shifts (δ) are reported in part per million (ppm) relative to the residual solvent peak. Column chromatography was performed on silica gel (70–230 mesh ASTM) using the reported eluents. Thin layer chromatography (TLC) was carried out on 5 x 20 cm plates with a layer thickness of 0.25 mm (Silica gel 60 F_{254}). When necessary they were developed with $KMnO_4$. Compounds **12**, **15** and **19** were analyzed by analytical reversed-phase Ultra High Performance Liquid Chromatography (RP-UHPLC) (Shimadzu Nexera liquid chromatograph LC- 30AD) equipped with a C18-bonded column (Phenomenex Kinetex, 150 mm × 4.6 mm, 5 μm, 100 Å), using isocratic 10% MeCN (0.1% TFA) in water (0.1% TFA) over 5 min, and gradient 10% to 90% elution of MeCN (0.1%

TFA) in water (0.1% TFA) over 15 min, with a flow rate of 1 mL/min and UV detection at 220 nm by a diode array UV−Vis detector. The purity of compounds was confirmed as ≥ 95%.

General procedure for the GBB-3CR (A-G). The nucleobase (adenine, guanine, or cytosine) (1 mmol, 1 eq.), the substituted benzaldehyde (1 mmol, 1 eq.) and the isocyanide (1 mmol, 1 eq.) were one-pot mixed in DMSO (2.5 mL, 0.4 M); the catalyst, $ZrCl_4$ (0.1 mmol, 0.1 eq.) was added and the reaction was stirred at 100 °C for 20 hours. The formation of the GBB-3CR adduct was monitored by TLC (typically dichloromethane/methanol 9:1), and the crude material was purified by column chromatography.

3-(*tert*-butylamino)-2-(4-(dimethylamino)phenyl)imidazo[1,2-*c*]pyrimidin-5(6*H*)-one (A). The crude material was purified by column chromatography (DCM/MeOH 95:5) to give the product as beige solid (88 mg, 27% yield). ^{1}H NMR (400 MHz, DMSO-d_6) δ 11.20 (br s, -N*H*), 7.92 (d, *J*= 7.2 Hz, 2H), 7.07-7.05 (m, 1H), 6.70-6.68 (m, 2H), 6.41-6.39 (m, 1H), 6.45 (br s, -N*H*), 2.90 (s, 6H), 0.95 (s, 9H). HRMS (ESI) *m/z* Calcd for $C_{18}H_{24}N_5O^+$: 326.1976; Found: 326.1976 $[M+H]^+$.

8-(*tert*-butylamino)-7-(4-chlorophenyl)-1*H*-imidazo[2,1-*b*]purin-4(5*H*)-one (B). The crude material was purified by column chromatography (DCM/MeOH 95:5) to give the product as amorphous solid (39 mg, 11% yield). ^{1}H NMR (400 MHz, DMSO-d_6) δ 12.21 (br s, -N*H*), 8.18 (s, 1H), 8.06 (d, *J*= 8.8 Hz, 2H), 7.37 (d, *J*= 8.8 Hz, 2H), 4.11 (br s, -N*H*), 1.03 (s, 9H). HRMS (ESI) *m/z* Calcd for $C_{17}H_{18}ClN_6O^+$: 357.1226; Found: 357.1229 $[M+H]^+$.

***N*-(*tert*-butyl)-8-(4-(dimethylamino)phenyl)-3*H*-imidazo[2,1-*i*]purin-7-amine (C).** The crude material was purified by column chromatography (DCM/MeOH 96:4) to give the product as yellowish solid (59 mg, 17% yield). ^{1}H NMR (400 MHz, DMSO-d_6) δ 8.95 (s, 1H), 8.20 (s, 1H), 8.03 (d, *J*= 8.4 Hz, 2H), 6.75 (d, *J*= 8.4 Hz, 2H), 4.61 (br s, -N*H*), 2.93 (s, 6H), 1.03 (s, 9H). HRMS (ESI) *m/z* Calcd for $C_{19}H_{24}N_7^+$: 350.2088; Found: 350.2087 $[M+H]^+$.

***N*-(*tert*-butyl)-8-(4-chlorophenyl)-3*H*-imidazo[2,1-*i*]purin-7-amine (D).** The crude material was purified by column chromatography (DCM/MeOH 97:3) to give the product as light orange solid (112 mg, 33%

yield). ^{1}H NMR (400 MHz, DMSO-d_6) δ 9.01 (s, 1H), 8.23-8.20 (m, 3H), 7.47 (d, *J*= 8.8 Hz, 2H), 4.79 (br s, -N*H*), 1.01 (s, 9H). HRMS (ESI) *m/z* Calcd for $C_{17}H_{18}ClN_6^+$: 341.1276; Found: 341.1273 $[M+H]^+$.

***N*-(*tert*-butyl)-8-(2-fluorophenyl)-3*H*-imidazo[2,1-*i*]purin-7-amine (E).** The crude material was purified by column chromatography (DCM/MeOH 95:5) to give the product as yellowish solid (162 mg, 50% yield). ^{1}H NMR (400 MHz, DMSO-d_6) δ 9.02 (br s, -N*H*), 7.93 (s, 1H), 7.75-7.72 (m, 1H), 7.40-7.35 (m, 1H), 7.29-7.26 (m, 2H), 7.19-7.14 (m, 1H), 5.25 (br s, -N*H*), 0.95 (s, 9H). HRMS (ESI) *m/z* Calcd for $C_{17}H_{18}FN_6^+$: 325.1572; Found: 325.1569 $[M+H]^+$.

2-(7-(*tert*-butylamino)-3*H*-imidazo[2,1-*i*]purin-8-yl)phenol (F). The crude material was purified by column chromatography (DCM/MeOH 95:5) to give the product as yellowish solid (116 mg, 36% yield). ^{1}H NMR (400 MHz, DMSO-d_6) δ 13.83 (br s, -N*H*), 11.74 (br s, -O*H*), 9.06 (s, 1H), 8.28 (s, 1H), 8.17-8.06 (m, 1H), 7.25-7.18 (m, 1H), 6.93-6.89 (m, 2H), 5.62 (br s, -N*H*), 1.04 (s, 9H). HRMS (ESI) *m/z* Calcd for $C_{17}H_{19}N_6O^+$: 323.1615; Found: 323.1613 $[M+H]^+$.

***N*-(*tert*-butyl)-8-(4-morpholinophenyl)-3*H*-imidazo[2,1-*i*]purin-7-amine (G).** The crude material was purified by column chromatography (DCM/MeOH 96:4) to give the product as white solid (74 mg, 19% yield). ^{1}H NMR (400 MHz, DMSO-d_6) δ 13.70 (br s, -N*H*), 8.97 (s, 1H), 8.21 (s, 1H), 8.10-8.05 (m, 2H), 6.97 (d, *J*= 8.4 Hz, 2H), 4.68 (br s, -N*H*), 3.75-3.73 (m, 4H), 3.17-3.14 (m, 4H), 1.03 (s, 9H). HRMS (ESI) *m/z* Calcd for $C_{21}H_{26}N_7O^+$: 392.2194; Found: 392.2188 $[M+H]^+$.

General procedure for the alkylation of GBB-3CR products. The GBB-3CR intermediate (**A-G**) (0.1 mmol, 1 eq.) was dissolved in DMF (0.33 mL, 0.3 M), the aminoalkyl halide (0.3 mmol, 3 eq.) and Cesium carbonate (0.5 mmol, 5 eq.) were added and the reaction was stirred overnight at 60 °C. The formation of the alkylated GBB-3CR product was monitored by TLC (typically dichloromethane/methanol 95:5 or 90:10), and the crude material was purified by column chromatography.

3-(*tert*-butylamino)-2-(4-(dimethylamino)phenyl)-6-(2-morpholinoethyl)imidazo[1,2-*c*]pyrimidin-5(6*H*)-one (4). The crude material was purified by column chromatography (DCM/MeOH 97:3) to give the product as reddish sticky (25 mg, 57% yield). ^{1}H NMR (400 MHz, CD_3OD) δ 7.93 (d, *J*= 8.0 Hz, 2H), 7.33

(br d, 1H), 6.69 (d, *J*= 8.0 Hz, 2H), 6.48 (br d, 1H), 4.48 (br s, 1H), 3.98-3.95 (m, 2H), 3.54-3.49 (m, 4H), 2.89 (s, 6H), 2.59-2.56 (m, 2H), 2.48-2.40 (m, 4H), 0.95 (s, 9H). HRMS (ESI) *m/z* Calcd for $C_{24}H_{35}N_6O_2^+$: 439.2816; Found: 439.2812 $[M+H]^+$.

8-(*tert*-butylamino)-7-(4-chlorophenyl)-1-(2-morpholinoethyl)-1*H*-imidazo[2,1-*b*]purin-4(5*H*)-one (5). The crude material was purified by column chromatography (DCM/MeOH 90:10) to give the product as yellowish solid (13 mg, 28% yield). ^{1}H NMR (400 MHz, CD_3OD) δ 8.06 (s, 1H), 7.96 (br d, AA'XX', 2H), 7.36 (br d, AA'XX', 2H), 4.60-4.57 (m, 2H), 3.64-3.61 (m, 4H), 2.85-2.82 (m, 2H), 2.52-2.50 (m, 4H), 1.05 (s, 9H). HRMS (ESI) *m/z* Calcd for $C_{23}H_{29}ClN_7O_2^+$: 470.2066; Found: 470.2067 $[M+H]^+$.

***N*-(*tert*-butyl)-8-(4-(dimethylamino)phenyl)-3-(2-morpholinoethyl)-3*H*-imidazo[2,1-*i*]purin-7-amine (6).** The crude material was purified by column chromatography (DCM/MeOH 95:5) to give the product as yellow solid (26 mg, 56% yield). ^{1}H NMR (400 MHz, DMSO-d_6) δ 8.95 (s, 1H), 8.23 (s, 1H), 8.03 (d, *J*= 8.8 Hz, 2H), 6.75 (d, *J*= 8.8 Hz, 2H), 4.66-4.63 (m, 3H), 3.46-3.44 (m, 4H), 2.93 (s, 6H), 2.92-2.89 (m, 2H), 2.50-2.48 (m, 4H), 1.03 (s, 9H). HRMS (ESI) *m/z* Calcd for $C_{25}H_{35}N_8O^+$: 463.2929; Found: 463.2922 $[M+H]^+$.

***N*-(*tert*-butyl)-8-(4-(dimethylamino)phenyl)-3-(2-(pyrrolidin-1-yl)ethyl)-3*H*-imidazo[2,1-*i*]purin-7-amine (7).** The crude material was purified by column chromatography (DCM/MeOH 90:10) to give the product as reddish amorphous solid (28 mg, 63% yield). ^{1}H NMR (400 MHz, DMSO-d_6) δ 8.94 (s, 1H), 8.24 (s, 1H), 8.04 (d, *J*= 8.8 Hz, 2H), 6.75 (d, *J*= 8.8 Hz, 2H), 4.64 (br s, -N*H*), 4.62-4.60 (m, 2H), 3.06-3.04 (m, 2H), 2.93 (s, 6H), 2.56-2.53 (m, 4H), 1.65-1.61 (m, 4H), 1.04 (s, 9H). HRMS (ESI) *m/z* Calcd for $C_{25}H_{35}N_8^+$: 447.2980; Found: 447.2976 $[M+H]^+$.

***N*-(*tert*-butyl)-8-(4-(dimethylamino)phenyl)-3-(3-(dimethylamino)propyl)-3*H*-imidazo[2,1-*i*]purin-7-amine (8).** The crude material was purified by column chromatography (DCM/MeOH 90:10) to give the product as reddish sticky solid (36.5 mg, 84% yield). ^{1}H NMR (400 MHz, DMSO-d_6) δ 8.95 (s, 1H), 8.20 (s, 1H), 8.04 (d, *J*= 8.4 Hz, 2H), 6.74 (d, *J*= 8.8 Hz, 2H), 4.64 (br s, -N*H*), 4.53-4.50 (m, 2H), 2.93 (s, 6H), 2.34-2.31 (m, 2H), 2.20 (s, 6H), 2.17-2.15 (m, 2H), 1.03 (s, 9H). HRMS (ESI) *m/z* Calcd for $C_{24}H_{35}N_8^+$: 435.2980; Found: 435.2975 $[M+H]^+$.

***N*-(*tert*-butyl)-8-(4-chlorophenyl)-3-(2-morpholinoethyl)-3*H*-imidazo[2,1-*i*]purin-7-amine (10).** The crude material was purified by column chromatography (DCM/MeOH 97:3) to give the product as yellowish solid (17 mg, 37% yield). ^{1}H NMR (400 MHz, DMSO-d_6) δ 9.01 (s, 1H), 8.27 (s, 1H), 8.21 (d, *J*= 8.8 Hz, 2H), 7.48 (d, *J*= 8.0 Hz, 2H), 4.82 (br s, -N*H*), 4.65 (m, 2H), 3.45-3.43 (m, 4H), 2.91-2.88 (m, 2H), 2.48-2.43 (m, 4H), 1.03 (s, 9H). HRMS (ESI) *m/z* Calcd for $C_{23}H_{29}ClN_7O^+$: 454.2117; Found: 454.2113 $[M+H]^+$.

***N*-(*tert*-butyl)-8-(4-chlorophenyl)-3-(2-(pyrrolidin-1-yl)ethyl)-3*H*-imidazo[2,1-*i*]purin-7-amine (11).** The crude material was purified by column chromatography (DCM/MeOH 90:10) to give the product as light orange solid (28 mg, 63.5% yield). ^{1}H NMR (400 MHz, DMSO-d_6) δ 9.00 (s, 1H), 8.27 (s, 1H), 8.22 (d, *J*= 8.0 Hz, 2H), 7.48 (d, *J*= 7.6 Hz, 2H), 4.82 (br s, -N*H*), 4.65-4.62 (m, 2H), 3.05-3.03 (m, 2H), 2.53-2.50 (m, 4H), 1.64-1.60 (m, 4H), 1.03 (s, 9H). HRMS (ESI) *m/z* Calcd for $C_{23}H_{29}ClN_7^+$: 438.2168; Found: 438.2166 $[M+H]^+$.

***N*-(*tert*-butyl)-8-(4-chlorophenyl)-3-(3-(dimethylamino)propyl)-3*H*-imidazo[2,1-*i*]purin-7-amine (12).** The crude material was purified by column chromatography (DCM/MeOH 90:10) to give the product as yellowish solid (25 mg, 59% yield). ^{1}H NMR (400 MHz, DMSO-d_6) δ 9.02 (s, 1H), 8.24-8.22 (m, 3H), 7.48 (d, *J*= 8.4 Hz, 2H), 4.83 (br s, -N*H*), 4.54-4.51 (m, 2H), 2.30-2.27 (m, 2H), 2.16 (s, 6H), 2.18-2.13 (m, 2H), 1.03 (s, 9H); ^{13}C NMR (100 MHz, DMSO-d_6) δ 148.3, 135.9, 134.3, 133.9, 132.2, 129.7, 128.5, 124.6, 113.7, 56.3, 56.2, 45.5, 45.4, 30.3, 28.2. HRMS (ESI) *m/z* Calcd for $C_{22}H_{29}ClN_7^+$: 426.2168; Found: 426.2164 $[M+H]^+$. t_R (min): 11.6.

***N*-(*tert*-butyl)-8-(2-fluorophenyl)-3-(2-morpholinoethyl)-3*H*-imidazo[2,1-*i*]purin-7-amine (13).** The crude material was purified by column chromatography (DCM/MeOH 97:3) to give the product as yellowish solid (18 mg, 42% yield). ^{1}H NMR (400 MHz, DMSO-d_6) δ 9.04 (s, 1H), 8.28 (s, 1H), 7.81-7.77 (m, 1H), 7.46-7.40 (m, 1H), 7.32-7.29 (m, 2H), 4.64-4.61 (m, 2H), 4.20 (br d, -N*H*), 3.43-3.41 (m, 4H), 2.89-2.86 (m, 2H), 2.45-2.41 (m, 4H), 0.91 (s, 9H). HRMS (ESI) *m/z* Calcd for $C_{23}H_{29}FN_7O^+$: 438.2413; Found: 438.2408 $[M+H]^+$.

***N*-(*tert*-butyl)-8-(2-fluorophenyl)-3-(2-(pyrrolidin-1-yl)ethyl)-3*H*-imidazo[2,1-*i*]purin-7-amine (14).** The crude material was purified by column chromatography (DCM/MeOH 90:10) to give the product as

reddish solid (29mg, 69% yield). ^{1}H NMR (400 MHz, DMSO-d_6) δ 9.04 (s, 1H), 8.28 (s, 1H), 7.83-7.79 (m, 1H), 7.46-7.41 (m, 1H), 7.33-7.28 (m, 2H), 4.62-4.59 (m, 2H), 4.19 (br s, -N*H*), 2.52-2.48 (m, 6H), 1.63-1.61 (m, 4H), 0.91 (s, 9H). HRMS (ESI) *m/z* Calcd for $C_{23}H_{29}FN_7^+$: 422.2463; Found: 422.2458 $[M+H]^+$.

***N*-(*tert*-butyl)-3-(3-(dimethylamino)propyl)-8-(2-fluorophenyl)-3*H*-imidazo[2,1-*i*]purin-7-amine (15).** The crude material was purified by column chromatography (DCM/MeOH 90:10) to give the product as amorphous solid (19 mg, 47% yield). ^{1}H NMR (400 MHz, DMSO-d_6) δ 9.04 (s, 1H), 8.24 (s, 1H), 7.83-7.79 (m, 1H), 7.46-7.42 (m, 1H), 7.31-7.28 (m, 2H), 4.51-4.48 (m, 2H), 4.19 (br s, -N*H*), 2.45-2.23 (m, 2H), 2.16-2.13 (m, 2H), 2.13 (s, 6H), 0.91 (s, 9H); ^{13}C NMR (100 MHz, DMSO-d_6) δ 160.0 (d, $J_{C\text{-}F}$ = 245.5 Hz), 148.1, 134.3, 133.5 (d, $J_{C\text{-}F}$ = 2.1 Hz), 132.2 (d, $J_{C\text{-}F}$ = 3.5 Hz), 130.4 (d, $J_{C\text{-}F}$ = 8.1 Hz), 125.7, 124.8 (d, $J_{C\text{-}F}$ = 3.2 Hz), 123.1 (d, $J_{C\text{-}F}$ = 14.1 Hz), 116.2 (d, $J_{C\text{-}F}$ = 21.8 Hz), 113.7, 56.1, 55.7, 45.5, 45.4, 30.0, 28.1. HRMS (ESI) *m/z* Calcd for $C_{22}H_{29}FN_7^+$: 410.2463; Found: 410.2460 $[M+H]^+$. t_R (min): 10.8.

***N*-(*tert*-butyl)-8-(2-(2-morpholinoethoxy)phenyl)-3-(2-morpholinoethyl)-3*H*-imidazo[2,1-*i*]purin-7-amine (16).** The crude material was purified by column chromatography (DCM/MeOH 95:5) to give the product as amorphous solid (17 mg, 31.5% yield). ^{1}H NMR (400 MHz, DMSO-d_6) δ 9.01 (s, 1H), 8.26 (s, 1H), 7.68 (d, *J*= 7.6 Hz, 1H), 7.36-7.32 (m, 1H), 7.16 (d, *J*= 8.4 Hz, 1H), 7.10-7.06 (m, 1H), 4.64-4.61 (m, 2H), 4.21 (br s, -N*H*), 4.15-4.13 (m, 2H), 3.51-3.43 (m, 8H), 2.89-2.86 (m, 2H), 2.62-2.60 (m, 2H), 2.48-2.44 (m, 4H), 2.35-2-34 (m, 4H), 0.90 (s, 9H). HRMS (ESI) *m/z* Calcd for $C_{29}H_{41}N_8O_3^+$: 549.3297; Found: 549.3297 $[M+H]^+$.

***N*-(*tert*-butyl)-8-(2-(2-(pyrrolidin-1-yl)ethoxy)phenyl)-3-(2-(pyrrolidin-1-yl)ethyl)-3*H*-imidazo[2,1-*i*]purin-7-amine (17).** The crude material was purified by column chromatography (DCM/MeOH 90:10) to give the product as yellowish solid (18 mg, 35% yield). ^{1}H NMR (400 MHz, DMSO-d_6) δ 8.99 (s, 1H), 8.27 (s, 1H), 7.70 (dd, *J*= 7.6, 1.6 Hz, 1H), 7.37-7.33 (m, 1H), 7.16-7.06 (m, 2H), 4.63-4.60 (m, 2H), 4.34 (br s, -N*H*), 4.15-4.13 (m, 2H), 3.07-3.04 (m, 2H), 2.80-2.78 (m, 2H), 2.55-2.49 (m, 8H), 1.67-1.62 (m, 8H), 0.88 (s, 9H). HRMS (ESI) *m/z* Calcd for $C_{29}H_{41}N_8O^+$: 517.3398; Found: 517.3393 $[M+H]^+$.

***N*-(*tert*-butyl)-8-(2-(3-(dimethylamino)propoxy)phenyl)-3-(3-(dimethylamino)propyl)-3*H*-imidazo[2,1-*i*]purin-7-amine (18).** The crude material was purified by column chromatography

(DCM/MeOH 50:50) to give the product as amorphous solid (11 mg, 22% yield). ^{1}H NMR (400 MHz, DMSO-d_6) δ 9.01 (s, 1H), 8.22 (s, 1H), 7.70 (dd, *J*= 7.2, 0.8 Hz, 1H), 7.36 (t, *J*= 7.2 Hz, 1H), 7.16 (d, *J*= 8.4 Hz, 1H), 7.08 (t, *J*= 7.2 Hz, 1H), 4.52-4.48 (m, 2H), 4.13-4.10 (m, 2H), 4.00 (br s, -N*H*), 2.28-2.25 (m, 4H), 2.19-2.17 (m, 2H), 2.14 (s, 6H), 2.05 (s, 6H), 1.85-1.79 (m, 2H), 0.90 (s, 9H). HRMS (ESI) *m/z* Calcd for $C_{27}H_{41}N_8O^+$: 493.3398; Found: 493.3405 $[M+H]^+$.

***N*-(*tert*-butyl)-3-(2-morpholinoethyl)-8-(4-morpholinophenyl)-3*H*-imidazo[2,1-*i*]purin-7-amine (19).** The crude material was purified by column chromatography (DCM/MeOH 96:4) to give the product as reddish sticky solid (34 mg, 68% yield). ^{1}H NMR (400 MHz, DMSO-d_6) δ 8.96 (s, 1H), 8.24 (s, 1H), 8.06 (d, *J*= 8.8 Hz, 2H), 6.98 (d, *J*= 8.8 Hz, 2H), 4.68 (br s, -N*H*), 4.66-4.63 (m, 2H), 3.75-3.72 (m, 4H), 3.47-3.44 (m, 4H), 3.16-3.14 (m, 4H), 2.91-2.88 (m, 2H), 2.50-2.46 (m, 4H), 1.03 (s, 9H); ^{13}C NMR (100 MHz, DMSO-d_6) δ 150.5, 147.7, 137.4, 134.0, 128.8, 125.6, 122.9, 114.6, 113.9, 66.6, 66.5, 58.4, 56.0, 53.6, 48.5, 44.0, 30.4. HRMS (ESI) *m/z* Calcd for $C_{27}H_{37}N_8O_2^+$: 505.3034; Found: 505.3032 $[M+H]^+$. t_R (min): 10.4.

***N*-(*tert*-butyl)-8-(4-morpholinophenyl)-3-(2-(pyrrolidin-1-yl)ethyl)-3*H*-imidazo[2,1-*i*]purin-7-amine (20).** The crude material was purified by column chromatography (DCM/MeOH 95:5) to give the product as reddish solid (33 mg, 67% yield). ^{1}H NMR (400 MHz, DMSO-d_6) δ 8.96 (s, 1H), 8.25 (s, 1H), 8.08 (d, *J*= 8.8 Hz, 2H), 6.98 (d, *J*= 8.8 Hz, 2H), 4.68 (br s, -N*H*), 4.65-4.62 (m, 2H), 3.75-3.73 (m, 4H), 3.16-3.14 (m, 4H), 3.06-3.03 (m, 2H), 2.57-2.41 (m, 8H), 1.65-1.59 (m, 4H), 1.03 (s, 9H). HRMS (ESI) *m/z* Calcd for $C_{27}H_{37}N_8O^+$: 489.3085; Found: 489.3083 $[M+H]^+$.

***N*-(*tert*-butyl)-3-(3-(dimethylamino)propyl)-8-(4-morpholinophenyl)-3*H*-imidazo[2,1-*i*]purin-7-amine (21).** The crude material was purified by column chromatography (DCM/MeOH 90:10) to give the product as reddish solid (23 mg, 48% yield). ^{1}H NMR (400 MHz, DMSO-d_6) δ 8.97 (s, 1H), 8.20 (s, 1H), 8.08 (d, *J*= 8.8 Hz, 2H), 6.97 (d, *J*= 9.2 Hz, 2H), 4.69 (br s, -N*H*), 4.53-4.50 (m, 2H), 3.74-3.72 (m, 4H), 3.16-3.14 (m, 4H), 2.33-2.30 (m, 2H), 2.19 (s, 6H), 2.17-2.15 (m, 2H), 1.03 (s, 9H). HRMS (ESI) *m/z* Calcd for $C_{26}H_{37}N_8O^+$: 477.3085; Found: 477.3082 $[M+H]^+$.

Synthesis of 3-(3-aminopropyl)-*N*-(*tert*-butyl)-8-(4-(dimethylamino)phenyl)-3*H*-imidazo[2,1-*i*]purin-7-amine (**22**). **9** (0.2 mmol, 1 equiv.) was dissolved in ethanol (2 mL, 0.1 M) and hydrazine hydrate (0.29 mL,

4.7 equiv.) was added. The reaction was stirred at reflux temperature for 2 hours, evaporated to dryness and purified by column chromatography to give **22** as a off-white amorphous solid (22 mg, 27% yield). ^{1}H NMR (400 MHz, DMSO-d_6) δ 8.96 (s, 1H), 8.25 (s, 1H), 8.04 (d, *J*= 7.6 Hz, 2H), 6.75 (d, *J*= 7.6 Hz, 2H), 4.65 (br s, -N*H*), 4.61-4.57 (m, 2H), 2.93 (s, 6H), 2.60-2.57 (m, 2H), 2.14-2.10 (m, 2H), 1.04 (s, 9H). HRMS (ESI) *m/z* Calcd for $C_{22}H_{31}N_8^+$: 407.2667; Found: 407.2664 $[M+H]^+$.

Synthesis of 1-(3-(7-(*tert*-butylamino)-8-(4-(dimethylamino)phenyl)-3*H*-imidazo[2,1-*i*]purin-3-yl)propyl)guanidine (23). 22 (0.06 mmol, 1 equiv.) was dissolved in a 2:1 mixture of THF/NH_4OH (0.6 mL, 0.1 M), 2-ethyl-2-thiopseudourea hydrobromide was added (0.26 mmol, 4 equiv.) and the reaction was stirred in a sealed tube at 70 °C. After 20 hours, 2-ethyl-2-thiopseudourea hydrobromide was again added (0.26 mmol, 4 equiv.), together with NH_4OH (0.2 ml, 0.3M) and the reaction was stirred at 70 °C for 48 h. The reaction was monitored by TLC (DCM/MeOH/NH_4OH 90:10:0.01). The product was precipitated with DCM and filtered under vacuum to give **23** as an off-white solid (10 mg, 38% yield). ^{1}H NMR (400 MHz, CD_3OD) δ 9.04 (s, 1H), 8.22 (s, 1H), 7.85 (d, *J*= 8.8 Hz, 2H), 6.87 (d, *J*= 8.8 Hz, 2H), 4.71-4.68 (m, 2H), 4.57 (br s, -N*H*), 3.00 (s, 6H), 3.33-3.27 (m, 2H), 2.42-2.35 (m, 2H), 1.05 (s, 9H). HRMS (ESI) *m/z* Calcd for $C_{23}H_{33}N_{10}^+$: 449.2885; Found: 449.2883 $[M+H]^+$.

Oligonucleotide synthesis and sample preparation. DNA sequences were synthesized at 5 μmol scale on an ABI 394 DNA/RNA synthesizer (Applied Biosystem) using standard β-cyanoethylphosphoramidite solid phase chemistry. After synthesis, oligonucleotides were detached from support and deprotected by treatment with concentrated ammonia aqueous solution at 55 °C for 12 h. The combined filtrates and washings were concentrated under reduced pressure, dissolved in water, and purified by high-performance liquid chromatography (HPLC) on a Nucleogel SAX column (Macherey-Nagel, 1000−8/46), using buffer A consisting of 20 mM KH_2PO_4/K_2HPO_4 aqueous solution (pH 7.0), containing 20% (v/v) CH_3CN, buffer B consisting of 1 M KCl, 20 mM KH_2PO_4/K_2HPO_4 aqueous solution (pH 7.0), containing 20% (v/v) CH_3CN, and a linear gradient from 0% to 100% B for 30 min with a flow rate 1 mL/min.[61] The fractions of the oligomers were successively desalted with Sep-pak cartridges (C-18). The isolated oligomer was proved to be >98% pure by NMR. In particular, the following oligonucleotides have been synthesized: the *BCL-2*

promoter sequence d(GGGCGCGGGAGGAATTGGGCGGG) (*BCL2*-G4), the *c-MYC* promoter sequence d(TGAGGGTGGGTAGGGTGGGTAA) (*c-MYC* G4), the *c-KIT1* sequence from the *c-KIT* oncogene promoter d(AGGGAGGGCGCTGGGAGGAGGG) (*c-KIT1* G4), the 23-mer truncation of human telomeric sequence d[TAGGG(TTAGGG)$_3$] (*Tel23* G4), and the 20-mer hairpin duplex-forming sequence d(CGAATTCGTTTTCGAATTCG) (*Hairpin 20-mer*). Oligonucleotides were dissolved in a 20 mM KCl, 5 mM KH_2PO_4 buffer (pH 7.0) to obtain 220 μM solutions, then annealed by heating to 95 °C for 5 min, followed by slow cooling to room temperature and storage overnight at 4 °C. The concentration of oligonucleotides was verified by UV adsorption measurements at 90 °C using appropriate molar extinction coefficient values ε (λ= 260 nm) calculated by the nearest neighbor model. [62]

Circular dichroism spectroscopy. Circular dichroism experiments were recorded on a Jasco J-815 spectropolarimeter equipped with a PTC-423S/15 Peltier temperature controller. Spectra were recorded at 20 °C in the wavelength range of 230−360 nm and averaged over three scans. A scan rate of 100 nm/min, with a 1 s response time and 1 nm bandwidth were used. For the CD experiments, 10 μM G-quadruplex DNAs and 15 μM duplex were used. The ligand stock solutions were 10 mM in DMSO. CD spectra of DNA/ligand mixtures were obtained by adding 10 molar equiv of ligands and recorded 10 min after ligand addition. All spectra were baseline corrected and analyzed using Origin 7.0 software. CD melting were carried out in the 20−100 °C temperature range at 1 °C/min heating rate by following changes of CD signal at the wavelengths of the maximum CD intensity (264 nm for *c-MYC*, *BCL2* and *c-KIT1* G4s, while the wavelengths of 287 and 280 nm were used for the telomeric G4 and the hairpin-20 mer, respectively). CD melting experiments were recorded in the absence and presence of ligands (10 molar equiv) added to the folded DNA structures. The melting temperatures (T_m) were determined from curve fit using Origin 7.0 software. ΔT_m values were determined as the difference in melting temperature between the DNAs with and without ligands. All experiments were performed in triplicate and the values reported are average of three measurements.

Biological experiments. *Cell cultures.* Human MCF-7 breast adenocarcinoma cells, human HCT-116 colorectal carcinoma cells, human A375 melanoma cells, human HaCaT keratinocytes, and human normal dermal fibroblasts (HDF) were grown as previously reported.[42] Under the same experimental conditions,

human T lymphoblastoid cell line (Jurkat, clone E6-1) were grown in RPMI supplemented with heat-inactivated 10% fetal bovine serum (FBS), 2.5 mM glutamine, 100 U/mL penicillin and 100 μg/mL streptomycin (Euroclone).

In vitro bioscreens for antiproliferative activity. The antiproliferative activity of compounds **12**, **15** and **19** was investigated through the estimation of a "cell survival index", arising from the combination of cell viability evaluation with cell counting.[63] Cells were inoculated in 96-microwell culture plates at a density of 10^4 cells/well (except HDF whose density was 10^3 cells/well) and allowed to grow for 24 h. The medium was then replaced with fresh medium and cells were treated for further 48h with a range of concentrations (5→100 μM) of the tested compounds, as indicated in each experiment, by using DMSO as vehicle at a final concentration of 0.5% v/v. Cell viability was evaluated using the MTT assay procedure, which measures the level of mitochondrial dehydrogenase activity using the yellow 3-(4,5-dimethyl-2-thiazolyl)-2,5-diphenyl-2*H*-tetrazolium bromide (MTT, Sigma) as substrate. The assay is based on the redox ability of living mitochondria to convert dissolved MTT into insoluble purple formazan. Briefly, after the treatments, the medium was removed and the cells were incubated with 20 μl/well of a MTT solution (5 mg/mL) for 1 h in a humidified 5% CO_2 incubator at 37 °C. The incubation was stopped by removing the MTT solution and by adding 100 μl/well of DMSO to solubilize the obtained formazan. Alternatively, for non-adherent Jurkat cells, after treatments 20 μl aliquots of MTT solution were added to each well and incubated for 1 h at 37°C in humidified 5% CO_2 following by low centrifugation at 800 rpm for 5 min. Then, 200 μl of the supernatant culture medium were carefully aspirated and 200 μl aliquots of DMSO were added to each well to dissolve the formazan crystals. Finally, the absorbance was monitored at 550 nm using a microplate reader (iMark microplate reader, Bio-Rad, Milan, Italy). Cell number was determined by TC20 automated cell counter (Bio-Rad, Milan, Italy), providing an accurate and reproducible total count of cells and a live/dead ratio in one step by a specific dye (trypan blue) exclusion assay. Bio-Rad's TC20 automated cell counter uses disposable slides, TC20 trypan blue dye (0.4% trypan blue dye w/v in 0.81% sodium chloride and 0.06% potassium phosphate dibasic solution) and a CCD camera to count cells based on the analyses of captured images. Once the loaded slide is inserted into the slide port, the TC20 automatically focuses on the cells, detects the

presence of trypan blue dye and provides the count. When cells are damaged or dead, trypan blue can enter the cell allowing living cells to be counted. Operationally, after treatments in 96-microwell culture plates, the medium was removed and the cells were collected. Ten microliters of cell suspension, mixed with 0.4% trypan blue solution at 1:1 ratio, were loaded into the chambers of disposable slides. The results are expressed in terms of total cell count (number of cells per ml). If trypan blue is detected, the instrument also accounts for the dilution and shows live cell count and percent viability. Total counts and live/dead ratio from random samples for each cell line were subjected to comparisons with manual hemocytometers in control experiments.[64] The calculation of the concentration required to inhibit the net increase in the cell number and viability by 50% (IC_{50}) is based on plots of data (n = 6 for each experiment) and repeated 3 times (total n = 18). IC_{50} values were obtained by means of a concentration response curve by nonlinear regression using a curve fitting program, GraphPad Prism 5.0, and are expressed as mean values ± SEM (n = 18) of five independent experiments.

Apoptosis experiments. The apoptosis assay was performed on Jurkat cells seeded at density of $1x10^6$ cells/well in a 6 well plate and incubated at 37 °C with molecules at 25 μM concentration. The apoptosis was analyzed after 48 h incubation by staining with annexin V/FITC and propidium iodine (PI) (eBioscience). Briefly, after incubation, the untreated and treated cells were detached with accutase solution (eBioscience), harvested and washed with cold PBS. Subsequently, the cells were treated following the manufacturer's instructions. The percentage of cell undergoing apoptosis or necrosis was quantified using a flow cytometer (Becton Dickinson) equipped with Cell Quest software.[50]

Western blotting. Jurkat cells were incubated with compounds **12**, **15** and **19** (25 μM) for 24 hours and then mechanically collected. Cells were lysate using lysis buffer (50 mM Hepes pH 7.4, 50 mM NaCl, 1% Triton) containing a protease inhibitor cocktail (Roche).[65] After 30 min incubation at 4 °C, cell lysates were centrifuged at 13.000 rpm for 30 min. Then, supernatants were separated from the cell debris and quantified by Bradford method using Bio-Rad reagent (Bio-Rad). Proteins were resolved by 10% SDS-polyacrylamide gel electrophoresis (SDS-PAGE) and blotted onto a nitrocellulose membrane (Bio-Rad). The membranes were incubated with primary antibodies (anti-Bcl-2, anti-*c*-Myc, and anti-β-actin, all from Sigma Aldrich)

over-night at 4°C. Subsequently, the membranes were incubated with peroxidase-conjugated goat anti-rabbit IgG for Bcl-2 protein immunodetection, or with peroxidase-conjugated goat anti-mouse IgG + IgM for *c*-Myc and β-actin (all the secondary antibodies were purchased from Jackson ImmunoResearch Laboratories). The resulting immunocomplexes were visualized by the ECL chemoluminescence method (Clarity™ Western ECL substrate, Bio-Rad Laboratories, US) and analyzed by an imaging system (ImageQuantTM400, GE Healthcare Life Sciences). Densitometric analysis was carried out using the GS-800 imaging densitometer (Bio-Rad). Normalization of results was ensured by incubating the nitrocellulose membranes in parallel with the β-actin antibody (Sigma-Aldrich).[66]

RT-PCR and qPCR. To perform total RNA extraction, treated cells were lysed with TRI Reagent (Sigma Aldrich). Successively, to obtain cDNA, a reverse transcription was performed using 0.5 μg of total RNA, 200 U of MMLV Reverse Transcriptase RNaseH- (Euroclone), dNTPs, random primers, RNase inhibitor. The reaction was conducted at 22 °C for 10 min and then at 42 °C for 60 min. The cDNA was subjected to qPCR assay using the primers: GAPDH forward 5'-AACGGGAAGCTTGTCATCAATGGAAA-3', GAPDH reverse 5'- GCATCAGCAGAGGGGGCAGAG-3'; *BCL2* Forward: 5'-CTGCACCTGACGCCCTTCACC-3'; *BCL2* Reverse: 5'-CACATGACCCCACCGAACTCAAAGA-3'; *c-MYC* Forward TTCGGGTAGTGGAAAACCAG; *c-MYC* Reverse: CAGCAGCTCGAATTTCTTCC (Sigma-Genosys). Reactions were carried out in duplicate. Quantitative PCR (qPCR) amplifications were achieved using the SYBR Premix Ex Taq II (Takara) in Rotor-gene Q (Qiagen). The qPCR protocol was as follows: 95 °C for 15 min followed by 40 cycles of 95 °C for 15 s, 59 °C for 30 s, and 72 °C for 30 s. Results were expressed as relative fold induction of the target genes relative to the reference gene. Calculations of relative expression levels were performed using the 2^{DDCt} method[67-68] and averaging the values of at least three independent experiments.

Microscale thermophoresis (MST) experiments. MST measurements were performed using the Monolith NT.115 (Nanotemper Technologies, Munich, Germany). The Cy5-fluorescently labeled *BCL2* and *c-MYC* oligonucleotides (Biomers) were prepared at 1 μM in 5 mM KH_2PO_4 buffer (pH 7.0) containing 20 mM KCl and annealed as described above. DNA samples were then diluted using the same phosphate buffer

supplemented with 0.1% Tween. For the MST experiments, the concentration of the labeled oligonucleotides was kept constant at 40 nM, while a serial dilution of the ligand (1:2 from 4 mM ligand stock solution in 100% DMSO) in the same buffer used for DNAs was prepared and mixed with the oligonucleotide solution with a volume ratio of 1:1. All the samples, containing 5% DMSO as the final concentration, were loaded into standard capillaries (NanoTemper Technologies). Measurements were performed and analyzed as previously reported.[52]

Nuclear Magnetic Resonance Experiments. NMR spectra were recorded on a Varian Unity INOVA 700 MHz spectrometer. One-dimensional proton spectra of samples in water were recorded using pulsed-field gradient DPFGSE for water suppression.[69] *BCL2* G4 and *c-MYC* G4 DNA samples was prepared at a concentration of 0.2 mM in 0.6 mL (H_2O/D_2O 9:1) buffer solution containing 5 mM KH_2PO_4, 20 mM KCl, 0.2 mM EDTA, at pH 7.0.[66] Aliquots of ligand stock solutions in deutero-DMSO (20 mM) were added directly to the DNA solution inside the NMR tube. The NMR data were processed on iMAC running iNMR software (www.inmr.net).

Molecular Modeling. All available crystal structures of *c-MYC* G4 and *BCL2* G4 were retrieved: PDB codes 1XAV, 2L7V, 5W77 and 2F8U respectively. Ligands and water molecules were removed; the binding site was detected using the original ligand coordinates, or the whole surface was considered. Ligand structure was built from a SMILES string and were minimized using Omega2.[70-72] The docking simulations were performed using FRED, and default settings were used and Chemgauss4 were considered as scoring function.[57] To validate the use of the FRED program, the docking studies were performed on the ligands in the considered crystal structures. FRED successfully reproduced the binding conformations reported in structure with acceptable root-mean-square deviation (rmsd < 1 Å) of atom coordinates. All structural images were prepared using PyMOL.[73]

Statistical data analysis. All data were presented as mean values ± SEM. The statistical analysis was performed using Graph-Pad Prism (version 6.01, Graph-Pad software Inc., San Diego, CA) and ANOVA test for multiple comparisons was performed followed by Bonferroni's test.

ASSOCIATED CONTENT

Supporting Information

CD spectra; NMR Tables of Δδ; Chemgauss4 values for *BCL2 G4* and *c-MYC* G4 structures; Copies of 1H- and 13C-NMR spectra; HR-MS spectra; HPLC Chromatograms (PDF). Molecular Formula Strings are provided as CSV file.

AUTHOR INFORMATION

Corresponding Author

*Mariateresa Giustiniano, mariateresa.giustiniano@unina.it

Author Contributions

# These authors contributed equally.

Funding Sources

The research of this manuscript was funded by AIRC (MFAG 18793).

Notes

The authors declare no competing financial interest.

ACKNOWLEDGMENT

This work was supported by the Italian Association for Cancer Research (AIRC; MFAG 18793 to M.G., IG 16730 to B.P., and IG 18695 to A.R.). Financial support from University of Naples Federico II and University of Piemonte Orientale, Novara, is also acknowledged.

ABBREVIATIONS

G4, G-Quadruplex; *BCL2*, B-cell lymphoma 2, CD, circular dichroism; MST, microscale thermophoresis; NMR, nuclear magnetic resonance; qPCR, quantitative polymerase chain reaction; GBB-3CR, Groebke-Blackburn-Bienaymé 3-Component Reaction; DMSO, dimethylsulfoxide; DMF, dimethyl formamide; HDF, human dermal fibroblasts; FITC, fluorescein isothiocyanate; PI, propidium Iodide; HPLC, high performance

liquid chromatography; HRMS, high resolution mass spectrometry; ESI, electrospray ionization; DCM, dichloromethane; MeOH, methanol.

REFERENCES

(1) Gellert, M.; Lipsett, M. N.; Davies, D. R. Helix Formation By Guanylic Acid. *Proc. Natl. Acad. Sci. U. S. A.* **1962**, *48*, 2013–2018.

(2) ClinicalTrials.gov, identifier: NCT00780663 (accessed Apr 8, 2019).

(3) Neidle, S. Therapeutic Applications of Quadruplex Nucleic Acids. 2012 Elsevier Inc. Academic Press, Amsterdam, Neth.

(4) Henderson, E.; Hardin, C. C.; Walk, S. K.; Tinoco, I.; Blackburn, E. H. Telomeric DNA Oligonucleotides Form Novel Intramolecular Structures Containing Guanine·Guanine Base Pairs. *Cell* **1987**, *51*, 899–908.

(5) Jain, A. K.; Bhattacharya, S. Interaction of G-Quadruplexes with Nonintercalating Duplex-DNA Minor Groove Binding Ligands. *Bioconjugate Chemistry* **2011**, *22*, 2355–2368.

(6) Maji, B.; Bhattacharya, S. Advances in the Molecular Design of Potential Anticancer Agents via Targeting of Human Telomeric DNA. *Chem. Commun.* **2014**, *50*, 6422–6438.

(7) Jain, A. K.; Paul, A.; Maji, B.; Muniyappa, K.; Bhattacharya, S. Dimeric 1,3-Phenylene-Bis(Piperazinyl Benzimidazole)s: Synthesis and Structure–Activity Investigations on Their Binding with Human Telomeric G-Quadruplex DNA and Telomerase Inhibition Properties. *J. Med. Chem.* **2012**, *55*, 2981–2993.

(8) Paul, A.; Maji, B.; Misra, S. K.; Jain, A. K.; Muniyappa, K.; Bhattacharya, S. Stabilization and Structural Alteration of the G-Quadruplex DNA Made from the Human Telomeric Repeat Mediated by Tröger's Base Based Novel Benzimidazole Derivatives. *J. Med. Chem.* **2012**, *55*, 7460–7471.

(9) Sundquist, W. I.; Klug, A. Telomeric DNA Dimerizes by Formation of Guanine Tetrads between Hairpin Loops. *Nature* **1989**, *342*, 825–829.

(10) Sun, D.; Thompson, B.; Cathers, B. E.; Salazar, M.; Kerwin, S. M.; Trent, J. O.; Jenkins, T. C.; Neidle, S.; Hurley, L. H. Inhibition of Human Telomerase by a G-Quadruplex-Interactive Compound. *J. Med. Chem.* **1997**, *40*, 2113–2116.

(11) Harrison, R. J.; Gowan, S. M.; Kelland, L. R.; Neidle, S. Human Telomerase Inhibition by Substituted Acridine Derivatives. *Bioorg. Med. Chem. Lett.* **1999**, *9*, 2463–2468.

(12) Selected general Reviews: Phan, A. T. Human Telomeric G-Quadruplex: Structures of DNA and RNA Sequences. *FEBS Journal* **2009**, *277*, 1107–1117; Neidle, S. Human Telomeric G-Quadruplex: The Current Status of Telomeric G-Quadruplexes as Therapeutic Targets in Human Cancer. *FEBS Journal* **2009**, *277*, 1118–1125; Lipps, H. J.; Rhodes, D. G-Quadruplex Structures: in Vivo Evidence and Function. *Trends in Cell Biology* **2009**, *19*, 414–422; Rhodes, D.; Lipps, H. J. G-Quadruplexes and Their Regulatory Roles in Biology. *Nucleic Acids Research* **2015**, *43*, 8627–8637; Ma, D.-L.; Zhang, Z.; Wang, M.; Lu, L.; Zhong, H.-J.; Leung, C.-H. Recent Developments in G-Quadruplex Probes. *Chemistry & Biology* **2015**, *22*, 812–828.

(13) Aboul-Ela, F.; Murchie, A. I. H.; Lilley, D. M. J. NMR Study of Parallel-Stranded Tetraplex Formation by the Hexadeoxynucleotide d(TG4T). *Nature* **1992**, *360*, 280–282.

(14) Simonsson, T.; Pecinka, P.; Kubista, M. DNA Tetraplex Formation in the Control Region of c-Myc. *Nucleic Acids Res.* **1998**, *26*, 1167–1172.

(15) Simonsson, T. G-Quadruplex DNA Structures Variations on a Theme. *Biol. Chem.* **2001**, *382*, 621-628.

(16) Neidle, S. Quadruplex Nucleic Acids as Novel Therapeutic Targets. *J. Med. Chem.* **2016**, *59*, 5987–6011.

(17) Siddiqui-Jain, A.; Grand, C. L.; Bearss, D. J.; Hurley, L. H. Direct Evidence for a G-Quadruplex in a Promoter Region and Its Targeting with a Small Molecule to Repress c-MYC Transcription. *Proc. Natl. Acad. Sci. U. S. A.* **2002**, *99* (18), 11593–11598.

(18) Agrawal, P.; Lin, C.; Mathad, R. I.; Carver, M.; Yang, D. The Major G-Quadruplex Formed in the Human BCL-2 Proximal Promoter Adopts a Parallel Structure with a 13-Nt Loop in K Solution. *J. Am. Chem. Soc.* **2014**, *136*, 1750–1753.

(19) Dai, J.; Chen, D.; Jones, R. A.; Hurley, L. H.; Yang, D. NMR Solution Structure of the Major G-Quadruplex Structure Formed in the Human BCL2 Promoter Region. *Nucleic Acids Res.* **2006**, *34*, 5133–5144.

(20) Membrino, A.; Cogoi, S.; Pedersen, E. B.; Xodo, L. E. G4-DNA Formation in the HRAS Promoter and Rational Design of Decoy Oligonucleotides for Cancer Therapy. *PLoS ONE* **2011**, *6*, e24421.

(21) Cogoi, S.; Paramasivam, M.; Spolaore, B.; Xodo, L. E. Structural Polymorphism within a Regulatory Element of the Human KRAS Promoter: Formation of G4-DNA Recognized by Nuclear Proteins. *Nucleic Acids Res.* **2008**, *36*, 3765–3780.

(22) Rankin, S.; Reszka, A. P.; Huppert, J.; Zloh, M.; Parkinson, G. N.; Todd, A. K.; Ladame, S.; Balasubramanian, S.; Neidle, S. Putative DNA Quadruplex Formation within the Humanc-KitOncogene. *J.Am.n Chem. Soc.* **2005**, *127*, 10584–10589.

(23) Fernando, H.; Reszka, A. P.; Huppert, J.; Ladame, S.; Rankin, S.; Venkitaraman, A. R.; Neidle, S.; Balasubramanian, S. A Conserved Quadruplex Motif Located in a Transcription Activation Site of the Human c-Kit Oncogene. *Biochemistry* **2006**, *45*, 7854–7860.

(24) Balasubramanian, S.; Hurley, L. H.; Neidle, S. Targeting G-Quadruplexes in Gene Promoters: a Novel Anticancer Strategy? *Nat. Rev. Drug Discov.* **2011**, *10*, 261–275.

(25) Drewe, W. C.; Nanjunda, R.; Gunaratnam, M.; Beltran, M.; Parkinson, G. N.; Reszka, A. P.; Wilson, W. D.; Neidle, S. Rational Design of Substituted Diarylureas: A Scaffold for Binding to G-Quadruplex Motifs. *J. Med. Chem.* **2008**, *51*, 7751–7767.

(26) Nasiri, H. R.; Bell, N. M.; Mcluckie, K. I. E.; Husby, J.; Abell, C.; Neidle, S.; Balasubramanian, S. Targeting a c-MYC G-Quadruplex DNA with a Fragment Library. *Chem. Commun.* **2014**, *50*, 1704–1707.

(27) Bugaut, A.; Jantos, K.; Wietor, J.-L.; Rodriguez, R.; Sanders, J. K. M.; Balasubramanian, S. Exploring the Differential Recognition of DNA G-Quadruplex Targets by Small Molecules Using Dynamic Combinatorial Chemistry. *Angew. Chem. Int. Ed.* **2008**, *47*, 2677–2680.

(28) Jana, S.; Panda, D.; Saha, P.; Pantoş G. Dan; Dash, J. Dynamic Generation of G-Quadruplex DNA Ligands by Target-Guided Combinatorial Chemistry on a Magnetic Nanoplatform. *J. Med. Chem.* **2018**, *62*, 762–773.

(29) Panda, D.; Saha, P.; Das, T.; Dash, J. Target Guided Synthesis Using DNA Nano-templates for Selectively Assembling a G-quadruplex Binding c-MYC Inhibitor. *Nat. Commun.* **2017**, *8*, 16103-16113.

(30) Ou, T.-M.; Lu, Y.-J.; Zhang, C.; Huang, Z.-S.; Wang, X.-D.; Tan, J.-H.; Chen, Y.; Ma, D.-L.; Wong, K.-Y.; Tang, J. C.-O.; Chan, A. S.-C.; Gu, L.-Q. Stabilization of G-Quadruplex DNA and Down-Regulation of Oncogene c-Myc by Quindoline Derivatives. *J. Med. Chem.* **2007**, *50*, 1465–1474.

(31) Ou, T.-M.; Lin, J.; Lu, Y.-J.; Hou, J.-Q.; Tan, J.-H.; Chen, S.-H.; Li, Z.; Li, Y.-P.; Li, D.; Gu, L.-Q.; Huang, Z.-S. Inhibition of Cell Proliferation by Quindoline Derivative (SYUIQ-05) through Its Preferential Interaction Withc-MycPromoter G-Quadruplex. *J. Med. Chem.* **2011**, *54*, 5671–5679.

(32) Liu, H.-Y.; Chen, A.-C.; Yin, Q.-K.; Li, Z.; Huang, S.-M.; Du, G.; He, J.-H.; Zan, L.-P.; Wang, S.-K.; Xu, Y.-H.; Tan, J.-H.; Ou, T.-M.; Li, D.; Gu, L.-Q.; Huang, Z.-S. New Disubstituted Quindoline Derivatives Inhibiting Burkitt's Lymphoma Cell Proliferation by Impeding c-MYC Transcription. *J. Med. Chem.* **2017**, *60*, 5438–5454.

(33) Chauhan, A.; Paul, R.; Debnath, M.; Bessi, I.; Mandal, S.; Schwalbe, H.; Dash, J. Synthesis of Fluorescent Binaphthyl Amines That Bind c-MYC G-Quadruplex DNA and Repress c-MYC Expression. *J. Med. Chem.* **2016**, *59*, 7275–7281.

(34) Zeng, D.-Y.; Kuang, G.-T.; Wang, S.-K.; Peng, W.; Lin, S.-L.; Zhang, Q.; Su, X.-X.; Hu, M.-H.; Wang, H.; Tan, J.-H.; Huang, Z.-S.; Gu, L.-Q.; Ou, T.-M. Discovery of Novel 11-Triazole Substituted Benzofuro[3,2-*b*]Quinolone Derivatives as c-Myc G-Quadruplex Specific Stabilizers via Click Chemistry. *J. Med. Chem.* **2017**, *60*, 5407–5423.

(35) Amato, J.; Morigi, R.; Pagano, B.; Pagano, A.; Ohnmacht, S.; De Magis, A.; Tiang, Y.P.; Capranico, G.; Locatelli, A.; Graziadio, A.; Leoni, A.; Rambaldi, M.; Novellino, E.; Neidle, S.; Randazzo, A. Toward the Development of Specific G-Quadruplex Binders: Synthesis, Biophysical, and Biological Studies of New Hydrazone Derivatives. *J. Med. Chem.* **2016**, *59*, 5706–5720.

(36) Hu, M.-H.; Wang, Y.-Q.; Yu, Z.-Y.; Hu, L.-N.; Ou, T.-M.; Chen, S.-B.; Huang, Z.-S.; Tan, J.-H. Discovery of a New Four-Leaf Clover-Like Ligand as a Potent c-MYC Transcription Inhibitor Specifically Targeting the Promoter G-Quadruplex. *J. Med. Chem.* **2018**, *61*, 2447–2459.

(37) Lavrado, J.; Borralho, P. M.; Ohnmacht, S. A.; Castro, R. E.; Rodrigues, C. M. P.; Moreira, R.; Daniel J. V. A. Dos Santos; Neidle, S.; Paulo, A. Synthesis, G-Quadruplex Stabilisation, Docking Studies, and Effect on Cancer Cells of Indolo[3,2-*b*]Quinolines with One, Two, or Three Basic Side Chains. *ChemMedChem* **2013**, 8, 1648-1661.

(38) Diveshkumar, K. V.; Sakrikar, S.; Harikrishna, S.; Dhamodharan, V.; Pradeepkumar, P. I. Targeting Promoter G-Quadruplex DNAs by Indenopyrimidine-Based Ligands. *ChemMedChem* **2014**, *9*, 2754–2765.

(39) Diveshkumar, K.V.; Sakrikar, S.; Rosu, F.; Harikrishna, S.; Gabelica, V.; Pradeepkumar, P. I. Specific Stabilization of c-MYC and c-KIT G-Quadruplex DNA Structures by Indolylmethyleneindanone Scaffolds. *Biochemistry* **2016**, *55*, 3571−3585.

(40) Rocca, R.; Moraca, F.; Costa, G.; Talarico, C.; Ortuso, F.; Ros, S. D.; Nicoletto, G.; Sissi, C.; Alcaro, S.; Artese, A. In Silico Identification of Piperidinyl-Amine Derivatives as Novel Dual Binders of Oncogene c-Myc/c-Kit G-Quadruplexes. *ACS Med. Chem. Lett.* **2018**, *9*, 848–853.

(41) Franceschin, M.; Cianni, L.; Pitorri, M.; Micheli, E.; Cacchione, S.; Frezza, C.; Serafini, M.; Hu, M.-H.; Su, H.; Huang, Z.; Gu, L.; Bianco, A. Natural Aromatic Compounds as Scaffolds to Develop Selective G-Quadruplex Ligands: From Previously Reported Berberine Derivatives to New Palmatine Analogues. *Molecules* **2018**, *23*, 1423-1436.

(42) Amato, J.; Pagano, A.; Capasso, D.; Di Gaetano, S.; Giustiniano, M.; Novellino, E.; Randazzo, A.; Pagano, B. Targeting the BCL2 Gene Promoter G-Quadruplex with a New Class of Furopyridazinone-Based Molecules. *ChemMedChem* **2018**, *13*, 406–410.

(43) Bejugam, M.; Sewitz, S.; Shirude, P. S.; Rodriguez, R.; Shahid, R.; Balasubramanian, S. Trisubstituted Isoalloxazines as a New Class of G-Quadruplex Binding Ligands: Small Molecule Regulation of c-Kit Oncogene Expression. *J. Am. Chem. Soc.* **2007**, *129*, 12926–12927.

(44) Dash, J.; Shirude, P. S.; Balasubramanian, S. G-Quadruplex Recognition by Bis-Indole Carboxamides. *Chem. Commun,* **2008**, 3055-3057.

(45) Pagano, B.; Cosconati, S.; Gabelica, V.; Petraccone, L.; Tito, S. D.; Marinelli, L.; Pietra, V. L.; Leva, F. S. D.; Lauri, I.; Trotta, R.; Novellino, E.; Giancola, C.; Randazzo, A. State-of-the-Art Methodologies for the Discovery and Characterization of DNA G-Quadruplex Binders. *Curr. Pharm. Des.* **2012**, *18*, 1880–1899.

(46) GBB MCR was first reported in 1998 by three independent research groups: Groebke, Blackburn and Bienaymé (a) Groebke, K.; Weber, L.; Mehlin, F. Synthesis of Imidazo[1,2-*a*] Annulated Pyridines, Pyrazines and Pyrimidines by a Novel Three-Component Condensation. *Synlett* **1998**, *1998*, 661–663.; (b) Blackburn, C.; Guan, B.; Fleming, P.; Shiosaki, K.; Tsai, S. Parallel Synthesis of 3-Aminoimidazo[1,2-*a*]Pyridines and Pyrazines by a New Three-Component Condensation. *Tetrahedron Lett.* **1998**, *39*, 3635–3638. (c) Bienaymé, H.; Bouzid, K. A New Heterocyclic Multicomponent Reaction For the Combinatorial Synthesis of Fused 3-Aminoimidazoles. *Angew. Chem. Int. Ed.* **1998**, *37*, 2234–2237.

(47) Guchhait, S. K.; Madaan, C. Groebke–Blackburn–Bienaymé Multicomponent Reaction in Scaffold-Modification of Adenine, Guanine, and Cytosine: Synthesis of Aminoimidazole-Condensed Nucleobases. *Tetrahedron Lett.* **2011**, *52*, 56–58.

(48) Merlino, F.; Yousif, A. M.; Billard, É.; Dufour-Gallant, J.; Turcotte, S.; Grieco, P.; Chatenet, D.; Lubell, W. D. Urotensin II(4–11) Azasulfuryl Peptides: Synthesis and Biological Activity. *J. Med. Chem.* **2016**, *59*, 4740–4752.

(49) Kendrick, S.; Muranyi, A.; Gokhale, V.; Hurley, L. H.; Rimsza, L. M. Simultaneous Drug Targeting of the Promoter MYC G-Quadruplex and BCL2 i-Motif in Diffuse Large B-Cell Lymphoma Delays Tumor Growth. *J. Med. Chem.* **2017**, *60*, 6587–6597.

(50) Reed, J. C.; Cuddy, M.; Haldar, S.; Croce, C.; Nowell, P.; Makover, D.; Bradley, K. BCL2-Mediated Tumorigenicity of a Human T-Lymphoid Cell Line: Synergy with MYC and Inhibition by BCL2 Antisense. *Proc. Natl. Acad. Sci.* **1990**, *87*, 3660–3664.

(51) Capasso, D.; Paola, I. D.; Liguoro, A.; Gatto, A. D.; Gaetano, S. D.; Guarnieri, D.; Saviano, M.; Zaccaro, L. RGDechi-HCit: αvβ3 Selective Pro-Apoptotic Peptide as Potential Carrier for Drug Delivery into Melanoma Metastatic Cells. *PLoS ONE* **2014**, *9*, e106441.

(52) Amato, J.; Platella, C.; Iachettini, S.; Zizza, P.; Musumeci, D.; Cosconati, S.; Pagano, A.; Novellino, E.; Biroccio, A.; Randazzo, A.; Pagano, B.; Montesarchio, D. Tailoring a Lead-like Compound Targeting Multiple G-Quadruplex Structures. *Eur. J. Med. Chem.* **2019**, *163*, 295–306.

(53) Entzian, C.; Schubert, T. Studying Small Molecule–Aptamer Interactions Using MicroScale Thermophoresis (MST). *Methods* **2016**, *97*, 27–34.

(54) Ambrus, A.; Chen, D.; Dai, J.; Jones, R. A.; Yang, D. Solution Structure of the Biologically Relevant G-Quadruplex Element in the Human *c*-MYC Promoter. Implications for G-Quadruplex Stabilization. *Biochemistry* **2005**, *44*, 2048–2058.

(55) Dai, J.; Carver, M.; Hurley, L. H.; Yang, D. Solution Structure of a 2:1 Quindoline–c-MYC G-Quadruplex: Insights into G-Quadruplex-Interactive Small Molecule Drug Design. *J. Am. Chem. Soc.* **2011**, *133*, 17673–17680.

(56) Calabrese, D. R.; Chen, X.; Leon, E. C.; Gaikwad, S. M.; Phyo, Z.; Hewitt, W. M.; Alden, S.; Hilimire, T. A.; He, F.; Michalowski, A. M.; Simmons, J. K.; Saunders, L. B.; Zhang, S.; Connors, D.; Walters, K. J.; Mock, B. A.; Schneekloth, J. S. Chemical and Structural Studies Provide a Mechanistic Basis for Recognition of the MYC G-Quadruplex. *Nat. Commun.* **2018**, *9* (1), 4229-4244.

(57) FRED 3.0.1: OpenEye Scientific Software, Santa Fe, NM. http://www.eyesopen.com (accessed Jun 21, 2019).

(58) Mcgann, M. FRED Pose Prediction and Virtual Screening Accuracy. *J. Chem. Inf. Model.* **2011**, *51*, 578–596.

(59) Laguerre, A.; Stefan, L.; Larrouy, M.; Genest, D.; Novotna, J.; Pirrotta, M.; Monchaud, D. A Twice-As-Smart Synthetic G-Quartet: PyroTASQ Is Both a Smart Quadruplex Ligand and a Smart Fluorescent Probe. *J. Am. Chem. Soc.* **2014**, *136*, 12406–12414.

(60) Kumar, Y. P.; Saha, P.; Saha, D.; Bessi, I.; Schwalbe, H.; Chowdhury, S.; Dash, J. Fluorescent Dansyl-Guanosine Conjugates that Bind *c*-MYC Promoter G-Quadruplex and Downregulate *c*-MYC Expression. *ChemBioChem* **2016**, *17*, 388–393.

(61) Pagano, B.; Amato, J.; Iaccarino, N.; Cingolani, C.; Zizza, P.; Biroccio, A.; Novellino, E.; Randazzo, A. Inside Cover: Looking for Efficient G-Quadruplex Ligands: Evidence for Selective Stabilizing Properties and Telomere Damage by Drug-Like Molecules. *ChemMedChem* **2015**, *10*, 640–649.

(62) Cantor, C. R.; Warshaw, M. M.; Shapiro, H. Oligonucleotide Interactions. III. Circular Dichroism Studies of the Conformation of Deoxyoligonucleolides. *Biopolymers* **1970**, *9*, 1059–1077.

(63) Irace, C.; Misso, G.; Capuozzo, A.; Piccolo, M.; Riccardi, C.; Luchini, A.; Caraglia, M.; Paduano, L.; Montesarchio, D.; Santamaria, R. Antiproliferative Effects of Ruthenium-based Nucleolipidic Nanoaggregates in Human Models of Breast Cancer In Vitro: Insights Into Their Mode of Action. *Sci. Rep.* **2017**, *7*, 45236.

(64) Santamaria, R.; Fiorito,F.; Irace, C.; De Martino, L.; Maffettone, C.; Granato, G. E.; Di Pascale, A.; Iovane, V.; Pagnini, U.; Colonna, A. 2,3,7,8-Tetrachlorodibenzo-p-dioxin Impairs Iron Homeostasis by Modulating Iron-related Proteins Expression and Increasing the Labile Iron Pool in Mammalian Cells. *Biochim. Biophys. Acta-Mol. Cell Res.* **2011**, *1813*, 704-712.

(65) Capasso, D.; Gaetano, S. D.; Celentano, V.; Diana, D.; Festa, L.; Stasi, R. D.; Rosa, L. D.; Fattorusso, R.; Dandrea, L. D. Unveiling a VEGF-Mimetic Peptide Sequence in the IQGAP1 Protein. *Mol. BioSyst.* **2017**, *13*, 1619–1629.

(66) Piccolo, M.; Misso, G.; Ferraro, M. G.; Riccardi, C.; Capuozzo, A.; Zarone, M. R.; Maione, F.; Trifuoggi, M.; Stiuso, P.; D' Errico, G.; Caraglia, M.; Paduano, L.; Montesarchio, D.; Irace, C.; Santamaria, R. Exploring Cellular Uptake, Accumulation and Mechanism of Action of a Cationic Ru-based Nanosystem in Human Preclinical Models of Breast Cancer. *Sci. Rep.* **2019**, *9*, 7006.

(67) Finetti, F.; Basile, A.; Capasso, D.; Gaetano, S. D.; Stasi, R. D.; Pascale, M.; Turco, C. M.; Ziche, M.; Morbidelli, L.; D'Andrea, L. D. Functional and Pharmacological Characterization of a VEGF Mimetic Peptide on Reparative Angiogenesis. *Biochem. Pharmacol.* **2012**, *84*, 303–311.

(68) Famiglini, V.; Coluccia, A.; Brancale, A.; Pelliccia, S.; Regina, G. L.; Silvestri, R. Arylsulfone-Based HIV-1 Non-Nucleoside Reverse Transcriptase Inhibitors. *Future Med. Chem.* **2013**, *5*, 2141–2156.

(69) Hwang, T.; Shaka, A. Water Suppression That Works. Excitation Sculpting Using Arbitrary Wave-Forms and Pulsed-Field Gradients. *J. Magn. Reson., Ser. A* **1995**, *112*, 275–279.

(70) Amato, J.; Pagano, A.; Cosconati, S.; Amendola, G.; Fotticchia, I.; Iaccarino, N.; Marinello, J.; Magis, A. D.; Capranico, G.; Novellino, E.; Pagano, B.; Randazzo, A. Discovery of the First Dual G-Triplex/G-Quadruplex Stabilizing Compound: a New Opportunity in the Targeting of G-Rich DNA Structures? *Biochim. Biophys. Acta (BBA) - General Subjects* **2017**, *1861*, 1271–1280.

(71) OMEGA, version 2.5.1.4; OpenEye Scientific Software: Santa Fe, NM; http://www.eyesopen.com (accessed Jun 21, 2019).

(72) Hawkins, P. C. D.; Skillman, A. G.; Warren, G. L.; Ellingson, B. A.; Stahl, M. T. Conformer Generation with OMEGA: Algorithm and Validation Using High Quality Structures from the Protein Databank and Cambridge Structural Database. *J. Chem. Inf. Model.* **2010**, *50*, 572–584.

(73) Hawkins, P. C. D.; Nicholls, A. Conformer Generation with OMEGA: Learning from the Data Set and the Analysis of Failures. *J. Chem. Inf. Model.* **2012**, *52* , 2919–2936.

(74) The PyMOL Molecular Graphics System, version 2.2.3; Schrödinger LLC: New York, 2018.

Table of Contents graphic